MacroTAC: Synthetic macrophage-targeting chimeras for targeted degradation of extracellular Pathological cargos

Zhengyu Ren[1, 2, #], Jiaxin Yu[3,4,#], Xiang-zheng Gao[3], Jintao Li[1, 2], Zikuan Zhao[5], Jingran Sun[1, 2], Tianyi Cheng[1, 2], Yingshan Jiang[1, 2], Ming-yue Wu[6], Yiting Wang[1, 2], Xu-xu Zhuang[1, 2], Run Han[1, 2], Wan Weng Ding[7], Erjin Wang[1, 2], Min Li[8], Maojin Yao[9,10], Jiaoyan Ren[4], Min Li[11], Ying Zheng[1, 2], Chen Ming[3, 4,*] Jia-Hong Lu[1, 2, 12, *]

[1]State Key Laboratory of Mechanism and Quality of Chinese Medicine, University of Macau, Macau SAR, China

[2]Institute of Chinese Medical Sciences, University of Macau, Macau SAR 999078, China

[3]Department of Public Health and Medicinal Administration, Faculty of Health Sciences (FHS), University of Macau, Macau SAR 999078, China

[4]Ministry of Education Frontiers Science Centre for Precision Oncology, University of Macau, Macau SAR 999078, China

[5]School of Food Sciences and Engineering, South China University of Technology, Guangzhou 510641, China

[6]Department of Gastroenterology, the First Affiliated Hospital (Southwest Hospital) of Third Military Medical University (Army Medical University), Chongqing 400038, China

[7]Center for Stem Cell Biology and Tissue Engineering, Key Laboratory for Stem Cells and Tissue Engineering, Ministry of Education, Sun Yat-Sen University, Guangzhou, 510080, China

[8]School of Pharmaceutical Sciences, State Key Laboratory of Anti-Infective Drug Discovery and Development, Guangdong Provincial Key Laboratory of Chiral Molecule and Drug Discovery, Sun Yat-Sen University, Guangzhou, Guangdong 510006, China

[9]Guangdong Provincial Key Laboratory of Malignant Tumor Epigenetics and Gene Regulation, Guangdong-Hong Kong Joint Laboratory for RNA Medicine, Medical Research Center, Sun Yat-Sen Memorial Hospital, Sun Yat-Sen University, Guangzhou 510120, China

[10]Nanhai Translational Innovation Center of Precision Immunology, Sun Yat-Sen Memorial Hospital, Foshan 528200, China

[11]Mr. & Mrs. Ko Chi-Ming Centre for Parkinson's Disease Research, School of Chinese Medicine, Hong Kong Baptist University, Hong Kong SAR 999077, China

[12]Guangdong-Hong Kong-Macau Joint Lab on Chinese Medicine and Immune Disease Research, University of Macau, Macau SAR 999078, China

[#]Co-First authors

[*]Correspondence: jiahonglu@um.edu.mo; chenming@um.edu.mo

Abstract

Targeted degradation strategies, such as PROTAC and LYTAC, have emerged as powerful tools for selective degradation of proteins or organelles. However, their applicability is restricted to intracellular cargos or limited number of extracellular proteins, leaving extracellular cargos such as pathogenic species, microbes, disease-associated protein aggregates, extracellular vesicles, cancer cells, and apoptotic cells, beyond the scope of these degraders. Here we developed MacroTAC (Macrophage-Targeting Chimera). a synthetic peptide-based platform designed to hijack the innate phagocytic capacity of macrophages for the clearance of cell-sized extracellular cargo. By engineering dual-headed peptides that simultaneously engage macrophage surface receptors (e.g., CD206) and disease-specific markers (e.g., calreticulin on apoptotic cells or EGFR on tumor cells), MacroTAC induces spatial proximity between macrophages and target cargo, thereby triggering precise and efficient phagocytosis. We validated this paradigm in two orthogonal disease models. In Dextran Sulfate Sodium Salt (DSS)-induced colitis, MacroTAC enhanced efferocytosis of apoptotic cells, reducing pathological burden and attenuating disease progression—an effect abolished in MerTK-deficient mice, confirming the dependence on canonical efferocytosis signaling. Crucially, single-cell RNA sequencing revealed that MacroTAC not only cleared cargo but also reprogrammed macrophages to remodel the immune microenvironment for sustainable therapeutic efficacy. In tumor xenografts, MacroTAC promoted macrophage-mediated phagocytosis of EGFR-high cancer cells, significantly suppressing tumor growth. By extending the induced-proximity principle beyond molecular degradation to cell-scale phagocytosis, MacroTAC establishes a versatile strategy for treating diseases driven by pathogenic extracellular cargo accumulation. This work bridges synthetic biology with innate immunity, offering a platform capable of targeting previously “undegradable” extracellular pathological structures.

Keywords:

induce proximity; macrophage-targeting chimeras; targeted degradation; efferocytosis; inflammatory bowel diseases; EGFR; lung cancer

Introduction

Inducing proximity principle provides a powerful tool to modulate the interaction between proteins for manipulating biological process, especially in the field of targeted protein degradation (TBD). By utilizing this principle, proteolysis targeting chimera (PROTAC) concept was proposed to design bi-head molecules for recruiting E3-ligase to transfer ubiquitin to protein of interest (POI) for its proteasomal degradation [1, 2]. This approach represents a paradigm shift in drug discovery, enabling the targeted degradation of previously undruggable disease-causing proteins and has now achieved initial clinical success [3]. Later, a series of lysosome-mediated targeted degradation strategies, such as the lysosome-targeting chimera (LYTAC) [4] and autophagy tethering chimera (ATTEC) [5-7], have been developed to selectively remove cargos that are not amenable to PROTAC-mediated degradation, including extracellular proteins, protein aggregates, surface receptors, and organelles [8]. Despite this progress, a critical gap remains in the elimination of even larger, cellular-scale pathogenic entities including pathogenic species that trigger infection, the apoptotic cell debris that perpetuates chronic inflammation, or even the entire tumor cells that form cancers, all of which are beyond the reach of current degraders.

Phagocytes, particularly macrophages, possess the evolved capacity to recognize and eliminate large cargoes via phagocytosis. This capability is not static but can be therapeutically induced. Genetic augmentation of efferocytosis, for instance by enhancing internalizing signals transduction, has been shown to markedly alleviate experimental colitis [9]; in oncology, blockade of the CD47 “don‘t eat me” signal with monoclonal antibodies enables macrophages to phagocytose tumor cells and has demonstrated clinical efficacy in multiple cancer types[10-12]. These studies provided definitive proof that modulation of phagocytotic activity of phagocytes is both achievable and therapeutically relevant. However, two major obstacles hinder the development of phagocytosis-targeting therapies: a scarcity of pharmacological tools to selectively regulate phagocytosis and the difficulty in achieving cargo-specific targeting. To meet these critical challenges, we developed a platform technology termed Macrophage-Targeting Chimera (MacroTAC). We proposed that a bifunctional peptide-based chimera, capable of simultaneously engaging a specific receptor on macrophages and a surface marker on unwanted extracellular cargos, could directionally recruit macrophages to induce phagocytosis and clearance of these cellular-sized cargoes.

Here, we conceptualized and validated MacroTAC using two parallel disease-relevant models: the enhancement of efferocytosis (phagocytosis of apoptotic cells) to resolve intestinal inflammation, and the direct phagocytosis of tumor cells for oncology applications. Taking advantage of versatility and engineerability of peptide, we designed and screened a series of dual-head peptides, and identified the MacroTACs that effectively motivate macrophages to uptake their intended

targets for lysosomal degradation in both *in vitro* and *in vivo* settings, alleviating disease pathology in murine models of colitis and cancer. Furthermore, we revealed that MacroTAC-mediated phagocytosis is not merely a clearance mechanism but also initiates profound reprogramming of the engaging macrophages, leading to sustained remodeling of the local immune microenvironment. This work establishes MacroTAC as a pioneering strategy that expands the therapeutic horizon of targeted degradation to the cellular-size extracellular cargos, offering a versatile platform for the treatment of a broad spectrum of diseases driven by extracellular pathological species.

Results

A synthetic approach identifies an efferocytosis-enhancing dual-head Macrophage-Targeting peptidic Chimera (effero-MacroTAC, eMacroTAC)

To design the MacroTAC for enhancing efferocytosis (Fig. 1a), we first retrieved the sequence of peptides that bind to the markers on macrophages and apoptotic cells through a systematic literature review. Five candidate peptides that bind to macrophage surface proteins (CD206 [13-16], TLR4 [17], CD11b [18], Fcγ receptor [19], and an unidentified target on M2 macrophages [20]), and two peptides that recognize phosphatidylserine (PS) [21, 22] or calreticulin (CRT)[23, 24] exposed on apoptotic cells were identified. These two groups of peptides were randomly conjugated via a flexible GSGS linker to generate a library of candidate effero-MacroTACs for functional screening (Fig. 1b). We established an *in vitro* efferocytosis assay by co-incubating mouse bone marrow-derived macrophages (BMDMs) with UV-induced apoptotic cells (ACs), and efferocytosis levels were quantified using high-content imaging (Extended data Fig. 1a). The expression level of corresponding proteins on the surface of macrophages or corpse was confirmed by cytometry (Extended data Fig. 1b-e). Since efferocytosis is a dynamic process encompassing corpse binding, internalization, and lysosomal degradation, we designed screening experiments to evaluate both binding and internalization/degradation. Apoptotic cells were labeled with either a pH-insensitive dye (celltraker-deepred) to track total cell binding or a pH-sensitive dye (pHrodo) that fluoresces upon lysosomal acidification to track the degradation process. From the ten candidate chimeras screened, the CD206-CRT bispecific peptide emerged as the top performer in both assays and was selected as effero-MacroTAC (eMacroTAC) for further characterization (Fig. 1c, d and Extended data Fig. 1f, g).

Microscale Thermophoresis (MST) was employed to confirm the direct binding between eMacroTAC and its purified protein targets. The eMacroTAC bound to the extracellular domain of CD206 with a Kd of 0.362 μM ± 0.047 μM and to CRT with a Kd of 0.118 μM ± 0.013 μM (Fig. 1e). Consistent with this, the eMacroTAC effectively enhanced the uptake of ACs by BMDMs at concentrations of 100 nM, 1

μM, and 10 μM (Extended data Fig. 1h). This enhancement was completely abrogated by blocking PS on the surface of apoptotic cells with Annexin V, indicating that the eMacroTAC induces a PS-dependent efferocytosis enhancement rather than non-specific phagocytosis (Fig. 1f). Similarly, the eMacroTAC did not promote BMDM phagocytosis of ether fluorescent microspheres or live cells (Extended data Fig. 2a, c). To pinpoint the stage of efferocytosis augmented by the eMacroTAC, we specifically inhibited the internalization step by treating BMDMs with cytochalasin D (Cyto D). Under this condition, the eMacroTAC still significantly increased the binding of ACs to BMDMs (Fig. 1g). Furthermore, eMacroTAC treatment did not alter general lysosomal acidity in BMDMs (Extended data Fig. 2d). These data collectively support that the eMacroTAC functions primarily as a molecular bridge that specifically promotes the initial recognition and binding of apoptotic cells to macrophages, rather than affecting downstream internalization or degradative machinery.

To further validate the target-specificity of this enhancement, we synthesized a scrambled-sequence control peptide. This peptide shared the same amino acid composition but with its CD206 and CRT targeting motif randomized (sc-MacroTAC), abolishing specific binding. In the efferocytosis assay, only the original eMacroTAC, but not the sc-MacroTAC enhanced BMDM engulfment (Fig. 1h). Moreover, this enhancement could be competitively inhibited by pre-treating cells with either the CRT-targeting peptide motif (CRTpep) or CD206 targeting peptide motif (CD206pep), confirming the requirement for specific, bifunctional engagement (Extended data Fig. 2i).

A critical concern when augmenting efferocytosis is that excessive corpse burden can overwhelm macrophage digestive capacity, leading to functional impairment. To determine whether eMacroTAC-enhanced binding disrupts subsequent degradative function, we performed a digestion assay. BMDMs were fed with lysosomal degradable dye CellTracker-labeled ACs in the presence or absence of eMacroTAC. After 1hr incubation, unbound ACs were washed away, and the fate of the internalized corpses was tracked. While eMacroTAC-treated BMDMs initially bound more ACs (as expected), these cells efficiently processed the increased load. The internalized corpses were progressively digested over time, and the excess burden was fully cleared within 36 hours, comparable to control conditions (Extended data Fig. 1j).

Next, we investigated the functional consequence of eMacroTAC-mediated efferocytosis enhancement on macrophage pro-resolution. The production of TGF-β and IL-10 upon eMacroTAC treatment was elevated (Fig. 1i, Extended data Fig. 1k). Consistent with this, RNA sequencing of macrophages following efferocytosis, with or without eMacroTAC treatment, revealed profound transcriptomic reprogramming. Gene set enrichment analysis (GSEA) indicated the upregulation

of pathways associated with efferocytosis including actin reorganization, calcium signaling, cell recognition, and cholesterol metabolism, and a concomitant downregulation of pro-inflammatory pathways such as IL-1 production, inflammatory response, NF-kappa B pathway, NO production, and TNF pathway (Extended data Fig. 3a-c). This demonstrated that eMacroTAC not only augments the clearance of apoptotic cells but also actively steers macrophages toward a resolution-promoting, anti-inflammatory phenotype.

Taken together, these data establish that the eMacroTAC functions as a specific molecular bridge, selectively enhancing the initial binding of ACs to macrophages via a dual-targeting mechanism and triggering subsequent pro-resolutive signaling in macrophages.

Effero-MacroTAC specifically binds to macrophages and ACs corpse via interacting with CD206 and calreticulin

To characterize the target binding properties of the eMacroTAC to its molecular targets, a Fluorescein isothiocyanate (FITC) conjugated eMacroTAC (FITC-eMacroTAC) and a scrambled-sequence control MacroTAC (FITC-sc-MacroTAC) were synthesized (Fig. 2a) to visualize the direct interaction between eMacroTAC and its target cells and investigated whether eMacroTAC binding to target cells is dependent on specific peptide sequence. Subsequently, we co-cultured BMDMs with or without CD206 expression induction (by IL-4 induction). Fluorescence imaging showed that FITC-eMacroTAC selectively bound to fixed BMDMs with high CD206 expression (stained with a CD206 specific antibody), while FITC-sc-MacroTAC did not showed such selectivity, confirming a correlation between receptor protein and chimera engagement. Critically, this binding could be competitively inhibited by pre-incubating of BMDMs with CD206-targeting peptide motif (Fig. 2b, c), suggesting a peptide sequence-dependent binding mode. Similarly, eMacroTAC binding to cells increased significantly upon induction of apoptosis and was specifically abolished by the CRT-targeting peptide motif (Fig. 2d-f), indicating a sequence-specific, CRT-dependent binding to apoptotic cells. This observation was also confirmed by flow cytometry (Fig. 2g).

Having hijacked CD206 for macrophages targeting, a critical question would be whether eMacroTAC will affect the innate function of CD206 as an important pathogen recognition receptor. We next sought to determine its interaction with CD206 in a native, live cellular context. Using live BMDMs, we aimed to determine whether eMacroTAC binding would trigger CD206 internalization, a key property of this endocytic receptor, and whether it would interfere with the receptor's function in pathogen recognition. Live-cell imaging revealed that FITC-eMacroTAC, unlike the FITC-sc-MacroTAC, remained stably associated with the macrophage surface membrane without be internalized (Fig. 2h). Subsequently, we quantified its direct equilibrium-binding affinity to both effector and target

cells using a flow cytometry-based cell surface binding assay [25] and the measured binding affinity for BMDMs was 0.3904 ± 0.111nM (Fig. 2i). Consistently, the Time-lapse imaging further showed that membrane-localized eMacroTAC was mobile. Upon addition of Cy5-labeled mannose, it rapidly co-accumulated with the ligand and was co-internalized, demonstrating that it does not impair the receptor's native endocytic function and can be co-trafficked with it (Fig. 2j-k). A flow cytometry-based mannose uptake assay using live macrophages confirmed that eMacroTAC pretreatment did not affect the capacity of macrophages to internalize the canonical ligand (Extended data Fig. 2e, f). Together, the eMacroTAC functions as a precision engager that stably and specifically docks onto the membrane of live macrophages without interfering with receptor's naïve function.

Effero-MacroTAC alleviates experimental colitis in mice model

Defective efferocytosis characterized by ACs accumulation in colon has been implicated in ulcerative colitis (UC) [26], and enhancement of efferocytosis displayed therapeutic potential against this chronic inflammatory disease [27, 28]. Pioneering work from Ravichandran et, al. showed the genetic enhancement of efferocytosis dramatically alleviated experimental colitis *in vivo*[9, 29, 30], and our previous work developed novel pharmacological tool to boost efferocytosis and resulted in experimental colitis alleviation [31, 32]. We observed massive CD206 positive macrophages infiltration in the inflamed colon tissue in DSS-induced colitis (Fig. 3a, b), which provides an ideal scenario to evaluate the therapeutic activity of eMacroTAC.

Prior to efficacy assessment, we characterized the pharmacokinetic (PK) profile of eMacroTAC. *In vivo* PK studies in mice revealed a plasma half-life of approximately 14.71 minutes, with FITC-eMacroTAC exhibiting shorter circulation than FITC-sc-MacroTAC, likely attributable to target engagement (Extended Data Fig. 4a, b). Despite rapid systemic clearance, FITC-eMacroTAC accumulated significantly in the colon under DSS-induced inflammatory conditions compared to the scrambled control (Extended Data Fig. 4c, d). More importantly, immunofluorescence staining confirmed that FITC-eMacroTAC exhibited marked CD206-specific targeting *in vivo*, with substantially higher accumulation on $CD206^+$ cells in the colon relative to sc-MacroTAC (Extended Data Fig. 4e). This efficient local targeting indicates that, despite rapid systemic clearance, eMacroTAC achieves engagement at the inflamed tissue site to exert therapeutic effects.

To evaluate the therapeutic efficacy of eMacroTAC *in vivo*, we established a DSS-induced colitis model with the following groups: normal (no treatment), PBS, sc-MacroTAC (1 mg/kg), eMacroTAC (1 mg/kg), CD206pep (5 mg/kg), and eMacroTAC (1 mg/kg) combined with CD206pep (5 mg/kg). Intravenous administration of eMacroTAC, but not sc-MacroTAC, significantly ameliorated key

colitis metrics, including body weight loss, disease activity index (DAI), colon shortening, and histological damage. This therapeutic effect was abolished by the competitive peptide CD206pep, indicating dependence on specific bridging effects (Fig. 3c-g) Consistent with this, eMacroTAC reduced the intestinal apoptotic cell burden and mitigated histological abnormalities, effects that were also attenuated by CD206 peptide blockade (Fig. 3f-i). These data collectively establish that the therapeutic benefit of eMacroTAC stems from its CD206-mediated bridging function. In addition, Intraperitoneal (*i.p.*) administration of eMacroTAC at both 1 mg/kg and 5 mg/kg effectively improved colitis symptoms (Extended Data Fig. 3 a-g). While both doses were effective, no statistically significant difference in therapeutic outcome was observed between them within this range, indicating a potential plateau effect within this dose range.

Single-cell RNA sequencing reveals that effero-MacroTAC promotes macrophages reprogramming *in vivo* and identifies MerTK as a key mediator of effero-MacroTAC-induced colitis alleviation

To gain deeper insight into the functional changes of macrophages during eMacroTAC-facilitated colitis resolution, we performed single-cell RNA sequencing (scRNA-seq) on cells isolated from the colons of PBS- and eMacroTAC-treated mice. Mice were administered 3.5% DSS in drinking water for 5 days, accompanied by daily intravenous injections of PBS or eMacroTAC (1 mg/kg) for 6 days. On day 6, mice were euthanized, and colonic cells were harvested for scRNA-seq analysis. An initial unbiased analysis of all colonic cell types from control group identified three functional distinct macrophages subtypes, Mac I represented more inflammatory response characters, Mac III represented a resolving property in contrast to Mac I, and Mac II represented the moderate type between Mac I and Mac III (Fig. 4a, b). We then compared the difference of all cell types between groups, eMacroTAC treatment led to a broad shift in the tissue landscape, notably, the epithelial cells, fibroblasts, and smooth muscle cells contents were significantly higher than control group, indicating a global pro-resolution response (Fig. 4c, Extended Data Fig. 6a). Consistently, the inflammatory Mac I was downregulated while resolving Mac III was upregulated by eMacroTAC treatment (Fig. 4d). UMAP visualization further confirmed a redistribution of macrophage subpopulations, with cell density shifting from the inflammatory type toward the resolving cluster in the eMacroTAC group compared with DSS controls (Fig. 4e, Extended Data Fig. 6b, c).

Directly observing efferocytosis *in vivo* within the complex colonic tissue presents a significant technical challenge. To overcome this and obtain molecular evidence for eMacroTAC's pro-efferocytic activity, we performed GSEA analysis to compare functional alterations induced by eMacroTAC on macrophages stratified by their expression levels of *Mrc1* (encoding CD206; the target of eMacroTAC). In macrophages with *Mrc1* expression (*Mrc1*$^{+}$), eMacroTAC treatment induced a

significant upregulation of efferocytosis related cellular events including binding (membrane adhesion molecules), ingesting (microvillus organization and actin filament-based movement etc.), suggesting a dramatic activation of efferocytosis. In contrast, *Mrc1*$^{-}$ macrophages showed no such alterations triggered by eMacroTAC, but enriched in antigen presentation related pathways (Fig. 4f-g). Consistent with the GSEA enrichment of phagocytosis-associated pathways in the eMacroTAC group, quantitative module score analysis demonstrated a significant increase in efferocytosis activity compared with DSS controls, with the enhancement being particularly prominent in *Mrc1*$^{+}$ macrophages (Fig. 4h). This provides compelling transcriptional evidence that eMacroTAC selectively activates the efferocytic program specifically in its target *Mrc1*$^{+}$ macrophage subset.

We next examined the expression of efferocytosis-related receptors in macrophages stratified by *Mrc1* expression. Within the *Mrc1*$^{+}$ subset, which represents the direct targets of eMacroTAC, we observed a significant upregulation of TAM family receptors, particularly *MerTK* (Fig. 4i, Extended Data Fig. 6c). This prompted us to investigate whether *MerTK* is functionally required for eMacroTAC's effects. Using bone marrow-derived macrophages (BMDMs) from *MerTK* knockout (KO) mice (Fig. 5a), we found that eMacroTAC completely lost its ability to enhance efferocytosis in *MerTK* KO BMDMs (Fig. 5b). The data is consistent with the previous observation that PS blockage by Annexin V abolished eMacroTAC-induced efferocytosis, indicating MerTK is required for eMacroTAC's pro-efferocytotic function. Crucially, this dependency translated to the *in vivo* setting, the protective effects of eMacroTAC against DSS-induced colitis were entirely abolished in MerTK-deficient mice (Fig. 5c-i,). Collectively, these data demonstrate that the downstream pro-resolving and therapeutic efficacy of eMacroTAC *in vivo* require efferocytosis receptor MerTK's function, suggesting an efferocytosis dependent anti-colitis activity.

Design and characterization of MacroTAC for tumor cells phagocytosis (tumor-MacroTAC, tMacroTAC)

To broaden the applicability of our platform and further validate the generalizability of the chimera concept, a tumor-targeting MacroTAC (tMacroTAC) has been designed. Given that tumor-associated macrophages (TAMs), which are a highly abundant immune population in the tumor microenvironment (TME), frequently express CD206, we retained the CD206-targeting moiety (CSPGAK). This motif was conjugated via a GSGS linker to a well validated EGFR-targeting peptide (YHWYGYTPQNVI) [33], generating the bispecific tMacroTAC (Fig. 6 a, b). EGFR is highly expressed in a wide range of cancer types, including lung cancer, thus we speculate that tMacroTAC will enhance the selective phagocytosis of EGFP positive cancer cells by macrophages.

The tMacroTAC bound directly to recombinant CD206 protein with an affinity of approximately 0.337 μM (Fig. 6c). Similar to eMacroTAC, FITC-tMacroTAC stably associated with the macrophage surface without inducing endocytosis, exhibiting a cellular binding affinity of about 0.5462 μM (Fig. 6d, e). The binding to BMDMs could be blocked by either an anti-CD206 antibody or CD206-targeting peptide motif CD206pep (Extended Data Fig. 7a), confirming the binding specificity. The chimera also bound to purified EGFR protein with high affinity (Kd ≈ 0.352 μM, Fig. 6g). We next evaluated the binding of tMacroTAC to live tumor cells in two cell lines with different EGFR expression level: HCC827 (high EGFR expression) and A549 (low EGFR expression) (Fig. 6f). Flow cytometry confirmed dose-dependent binding to both cell lines, with affinities of approximately 0.881 μM for HCC827 and 1.882 μM for A549 (Fig. 6h and Extended Data Fig. 7b). The subsequent FL staining showed co-localization of FITC-tMacroTAC with EGFR on the cell surface, and binding was abolished upon EGFR knockdown (Fig. 6i and Extended Data Fig. 7c), indicating a high specificity of EGFR targeting.

For functional validation, we used an anti-CD47 antibody (B6H12) to block the “don’t eat me” signal mediated by CD47 on tumor cells [11, 34], and then measured of phagocytosis of tumor cells by macrophages in a co-culture system. An initial imaging-based assay (as shown in Extended Data Fig. 1a, b) indicated that tMacroTAC could further enhance phagocytosis of tumor cells compared with that of CD47 antibody blockade alone (Extended Data Fig. 7d). We then employed a flow cytometry-based phagocytosis assay for accurate quantification (Extended Data Fig. 7e). tMacroTAC significantly enhanced the phagocytosis of EGFR-high HCC827 cells by BMDMs (Fig. 6j). Internalized tumor cells were subsequently transported to lysosome for degradation (Fig. 6k) and were effectively processed as confirmed by live cell imaging (Extended Data Fig. 7f and g). This enhancement was competitively inhibited by the CD206-targeting peptide motif (Fig. 6l). The pro-phagocytic effect of tMacroTAC in the presence of CD47 antibody was also observed on other EGFR-expressing cell lines, including A549 and NCI-H1975 (Extended Data Fig. 8a-e), confirming broad efficacy of tMacroTAC across cells with different EGFR mutational statuses (HCC827: exon 19 del; NCI-H1975: L858R; A549: wild-type). In contrast, no enhancement was observed against EGFR-negative Jurkat cells (Extended Data Fig. 8f), suggesting EGFR expression is indispensable to the pro-phagocytotic function of tMacroTAC. To rigorously validate EGFR-dependence of t MacroTAC, we knocked down (KD) the expression of EGFR on HCC827 cell line by shRNA (Extended Data Fig. 8g), and observed the complete abolishment of pro-phagocytic effect of tMacroTAC on EGFR-KD HCC827 cells (Fig. 6m, Extended Data Fig. 8h). Reversely, the pro-phagocytic effect of tMacroTAC was restored upon re-expression of wild-type EGFR in KD cells (Fig. 6n, Extended Data Fig. 8i). Consistent results were obtained with EGFR-KD NCI-H1975 cells (Fig. 6o, Extended Data Fig. 8j), confirming that the pro-phagocytic function of tMacroTAC is strictly dependent on EGFR expression on the tumor cell.

To sum up, the tumor-MacroTAC selectively enhances the macrophages phagocytosis of tumor cells simultaneously engaging CD206 on macrophages and EGFR on tumor cells. It thus validates the generalizability of the MacroTAC platform and underscores its potential to redirect TAMs for tumor cell clearance.

Tumor-MacroTAC inhibits tumor growth in a xenograft model

The anti-tumor effect of tMacroTAC combined with anti-CD47 antibody (Combo) was evaluated in HCC827 xenograft tumor model. Nude mice were subcutaneously inoculated with HCC827 cells. After tumor formation, mice were intratumorally administrated with tMacroTAC (1 mg/kg) every 2 or 3 days and intraperitoneally injected with CD47 antibody (200 μg/mice) every 2 or 3 days as indicated in Fig. 7a. Monitoring of tumor growth revealed that injection with anti-CD47 antibody at the experimental dosage seems no obvious inhibition to this tumor growth (Fig. 7b, red curve), but tMacroTAC alone treatment showed better effects than anti-CD47 antibody (Fig. 7b, blue curve); as expected, the combination of tMacroTAC with anti-CD47 antibody resulted in significantly greater tumor suppression compared to either agent alone (Fig. 7b, pink curve). Meanwhile, the combinatorial effect was partially reversed by co-administration of the competitive CD206-targeting peptide (Fig. 7b, green curve). Consistent with the growth curves, the macroscopic photographs and tumor weights showed that combo treatment further shrunk the tumor size, and that the competitive peptide CD206pep attenuated this efficacy (Fig. 7c). Importantly, the tMacroTAC and CD47 antibody did not cause obvious toxicity on mice (Extended Data Fig. 9a, b). These results indicated that tMacroTAC augments the anti-tumor activity of anti-CD47 antibody, primarily through its intended bridging mechanism. However, the observation that tMacroTAC alone treatment already suppressed tumor growth and competitive peptide only partially attenuated the tumor suppression activity of combo treatment (Fig. 7b, c), suggesting that tMacroTAC possessed unexpected, bridging-independent anti-tumor effects.

To elucidate the mechanistic basis for tumor growth inhibition, we assessed markers of cell death and proliferation *in situ*. Mice receiving the anti-CD47 antibody (either alone or in combination) exhibited increased cleaved caspase-3 staining. This antibody-dependent induction of cell death was further enhanced in the combination group, an effect that was effectively blocked by the competitive peptide (Fig. 7d-g). The data suggests that the tMacroTAC bridge not only promotes phagocytosis but may also potentiate antibody-dependent cellular cytotoxicity (ADCC).

Neutrophils within the tumor microenvironment (TME) are also capable of mediating ADCC. Immune staining revealed a notable spatial association between dying tumor cells and infiltrating neutrophils, specifically in the combination therapy group (Extended Data Fig. 9c). Interestingly, neutrophil infiltration was

also increased in the anti-CD47 antibody group and was further enhanced by tMacroTAC treatment, suggesting a phagocytosis-associated recruitment of neutrophil (Extended Data Fig. 9d, e). Previous study indicated that CD47 antibody-mediated tumor cell phagocytosis can induce a program of chemokine production in macrophages, including MCP-3 (CCL7) a potent neutrophil chemoattractant [12]. Immunofluorescence staining confirmed that CCL7 production within tumors followed a pattern highly consistent with neutrophil infiltration and was co-localized with macrophages (Extended Data Fig. 9f, g), suggesting a potential mechanism for the observed neutrophil recruitment.

Separately, a reduction in Ki67-positive cells was observed in all groups treated with tMacroTAC (monotherapy and combination). Notably, this anti-proliferative effect was not fully reversed by the competitive CD206 peptide (Fig. 7g), indicating it may stem from a direct, bridging-independent activity of the chimera. However, tMacroTAC treatment neither induced polarization of BMDM (Extended Data Fig. 9h, i), a process associated with tumor suppression [35], nor caused toxicity on tumor cells (Extended Data Fig. 9j, k).

Tumor-MacroTAC inhibits the proliferation of tumor cells harboring EGFR mutations

The EGFR-targeting peptide moiety (YHWYGYTPQNVI) has been reported to act as a competitive inhibitor of EGF binding, a step required for receptor dimerization and downstream pathway activation [36, 37]. Given that cells harboring EGFR mutations exhibit enhanced EGF-dependent signaling, which drives proliferation and survival, we hypothesized that tMacroTAC could suppress tumor growth by competitively inhibiting this ligand-dependent activation (Extended Data Fig. 10a). This hypothesis was validated in two parallel proliferation assays, the EdU incorporation (Fig. 7h) and CFSE dilution (Fig. 7i). As predicted, tMacroTAC significantly suppressed the EGF-driven proliferation of HCC827 cells in a dose-dependent manner. This finding was further confirmed by a clonogenic formation assay (Extended Data Fig. 10b). Meanwhile, tMacroTAC failed to inhibit the proliferation of EGFR-KD cells, regardless of EGF stimulation (Extended Data Fig. 10c). Notably, re-expression of wild-type EGFR in these KD cells did not restore sensitivity to tMacroTAC-mediated inhibition (Extended Data Fig. 10d), and clonogenic assays yielded consistent results (Extended Data Fig. 10e, f). This suggested that the anti-proliferative activity might depend not only on EGFR expression but also on its mutational status. Supporting this notion, tMacroTAC effectively inhibited the EGF-dependent growth of both a primary lung cancer cell line engineered to overexpress the human EGFR-L858R mutant and the endogenously L858R-mutant NCI-H1975 cell line (Extended Data Fig. 10g, h). In contrast, no significant inhibition was observed in EGFR-KD NCI-H1975 cells or in the H1299 cell line, which carries wild-type EGFR (Extended Data Fig. 10i, j).
Together, these findings demonstrate that tMacroTAC not only promoted

macrophages-mediated tumor cells phagocytosis through the induced spatial proximity but also exert a bridging-independent anti-proliferative effect on tumor cells by competitively inhibiting EGF-dependent EGFR signaling on tumor cells harboring oncogenic EGFR mutations.

Discussion

In this study, we established the Macrophage-Targeting Chimera (MacroTAC) as a pioneering platform that expands the therapeutic paradigm of induced proximity from molecular and organellar degradation to the clearance of cellular-scale pathological cargoes. By designing bifunctional peptides that bridge specific receptor CD206 on macrophages to surface markers on targeted cargos such as CRT on apoptotic cells and EGFR on tumor cells, we provide a targeting strategy to directionally recruit macrophages and enhance their intrinsic ability to recognize and engulf pathological cargoes that otherwise exacerbate disease conditions, such as apoptotic debris in inflammation, tumor cells in cancer, and potentially microbes or protein aggregates in other pathologies. This represents a significant conceptual leap, moving beyond recruiting intracellular degradation machinery to orchestrating a professional phagocyte for targeted clearance.

This conceptual framework also clarifies how MacroTAC relates to, yet fundamentally differs from emerging molecular-glue platforms. The principle of recruiting phagocytes via induced proximity is gaining traction recently, for instance, Morimoto *et al.* designed a TAM-targeting LYTAC (TICTAC) to degrade immune checkpoint receptors such as SIRPα, potentially enhancing tumor cell phagocytosis [38]; Du *et al.* developed a bispecific antibody-based engager (FcRTAC) to redirect microglia for extracellular beta-amyloid clearance, showing therapeutic efficacy in an Alzheimer's disease model [39]. Notably, both TICTAC and FcRTAC remain extensions of the LYTAC paradigm, relying on the chimera to directly trigger endocytic degradation of membrane proteins or protein aggregates. In contrast, MacroTAC is fundamentally designed to bridge macrophages to entire cells such as apoptotic and tumor cells, leveraging the cell's native, signal-integrated phagocytic machinery for phagocytic elimination. While antibody- or glycoconjugate-based designs like TICTAC and FcRTAC may offer high target affinity and efficient internalization, our peptide-based MacroTAC presents advantages in tissue permeability, low immunogenicity, and synthetic simplicity. Moreover, beyond mere clearance, we demonstrate that MacroTAC engagement actively reprograms the local immune microenvironment across both tumor and inflammatory disease contexts, revealing a previously unappreciated dimension of therapeutic potential.

Beyond this conceptual positioning, several design-specific insights emerge from our data. First, although both MacroTAC and reported LYTAC require lysosome for degradation, the key distinction lies in its mechanism of action. LYTACs function

by hijacking receptor endocytosis and vesicle trafficking pathways, directly causing internalization of their bound cargo. In contrast, we found that MacroTAC does not trigger constitutive internalization of its engaged receptor; it is stably retained on the macrophage surface without inducing endocytosis of CD206. Meanwhile, It preserves the normal function of CD206 for mannose-receptor-mediated antimicrobial activity, thus minimize off-target sequestration of the receptor in the absence of intended cargo. This cargo-specific conditional activation, an emergent property of the MacroTAC, may offer important advantages. Whether a version engineered to actively drive receptor internalization would enhance or compromise therapeutic efficacy remains an open question for future investigation.

Secondly, we observed a notable dissociation between the moderate enhancement of phagocytosis in isolated *in vitro* assays and the robust therapeutic efficacy achieved *in vivo*. We posit that this discrepancy underscores a profound immune-remodeling capacity intrinsic to the MacroTAC strategy. In the context of efferocytosis, eMacroTAC not only cleared apoptotic cells but also promoted a sustained pro-resolutive phenotype of macrophages, enabling continual efferocytosis and inflammation alleviation. In the xenograft tumor model, tMacroTAC-mediated phagocytosis was associated with enhanced chemokine secretion, such as MCP-3, and increased neutrophil recruitment, which spatially correlated with tumor cell death *in situ*. Thus, MacroTAC operates not merely as a simple bridge but as an engager of a post-phagocytic immune response, reprogramming the local microenvironment to sustain therapeutic effects, which is a layer of complexity absent in simpler *in vitro* phagocytosis assays.

Thirdly, we also uncovered an unexpected function of the tMacroTAC that operates independently of its bridging mechanism. Its EGFR-targeting motif competitively inhibited EGF-induced tumor cell proliferation. This finding reveals the multi-functional potential of peptide-based engagers but also raises new mechanistic questions. Specifically, the precise mode of tMacroTAC-mediated EGFR signaling suppression, such as via steric hindrance, disruption of receptor dimerization, or altered trafficking, remains to be elucidated.

The limitations of the current study warrant mention. The pharmacokinetic profile of the peptide-based MacroTACs is suboptimal, this is the common problem of peptide-based molecules, necessitating strategies for half-life extension such as amino acid substitution and Polyethylene glycol modification (PEGlation) for translational development. Beyond pharmacokinetics, the targeting motifs utilized in this study were retrieved from literature; although their targeting capability and *in vivo* performance have been carefully validated, there remains potential for further optimization to improve the binding affinity and stability. A further consideration is the broad tissue distribution of macrophages, which raises the question of whether MacroTAC accumulation at non-target sites could be

mitigated through disease-specific personalization strategies. Finally, the long-term fate and activation state of macrophages following repeated MacroTAC administration remain unclear and require longitudinal investigation to fully assess the safety and durability of this therapeutic approach.

Method

Animals

The Wild-type male C57BL/6J mice and Nude mice were purchased from the animal facility of the Faculty of Health Sciences of University of Macau. The MerTK KO mice were generated by Shanghai Model Organisms Center, Inc. and were genotyped by PCR with a forward primer (5'-GCTCTCCCAGCCTTGTCTTT-3') and reverse primer (5'-CCTGGACTACCTGAGAGCCT-3'). Mice were housed under controlled temperature (25°C) on 12 h light–dark cycles, with *ad libitum* access to food and water. All animal procedures were conducted at the University of Macau using guidelines approved (UMARE-023-2021; UMARE-034-2024).

Antibodies and Reagents

FITC anti-mouse/human CD11b Antibody (1:200, 101206), APC anti-mouse Tim-4 Antibody (1:200, 130021), PE anti-human CD47 Antibody (1:200, 323108), APC anti-mouse F4/80 Antibody (1:200, 123116), PerCP/Cyanine5.5 anti-mouse F4/80 Antibody (1:200, 123128), PE/Cyanine7 anti-mouse CD206 (MMR) Antibody (1:200, 141720) antibodies were purchased from BioLegend (CA, USA). F4/80 (BM8.1) Rat Monoclonal Antibody (1:500, 71299S), CD206/MRC1 (E6T5J) Rabbit Monoclonal Antibody (1:200, 24595S), EGF Receptor (D38B1) Rabbit Monoclonal Antibody (1:1000, 4267S), Cleaved Caspase-3 (1:500, Asp175) (5A1E) Rabbit Monoclonal Antibody (9664S), Ki-67 (D3B5) Rabbit Monoclonal Antibody (1:500, 9129S) antibodies were purchased from Cell Signaling Technology (MA, USA). MCP3 Polyclonal Antibody (bs-1987R) antibody was purchased from Bioss Inc (MA, USA). Goat anti-Mouse IgG cross-adsorbed secondary antibody (1:200, A21422), and anti-F4/80 (1:1,000, 14-4801-82) antibodies were purchased from ThermoFisher Scientific (MA, USA). Anti-GAPDH (1:3,000, AC001), anti-b-Actin (1:3,000, AC026), HRP Goat anti-Rabbit IgG (1:10,000, AS014), and HRP Goat anti-Mouse IgG (1:10,000, AS003) antibodies were purchased from ABclonal Technology (Wuhan, China). MerTK (AF591) was bought from R&D Systems.

All the peptide used in this study was synthesized by ChinaPeptides Co., Ltd. RNAiso Plus (NO.9108) was purchased from Takara (Kusatsu, Shiga, Japan). LysoTracker Red (L7528), pHrodo red/green AM (P35372/P35373), CellTracker Deepred (A66460), CellTracker Green CMFDA (A66461), CFSE (C34570), cytochalasin D (PHZ1063), and FluoSpheresTM Fluorescent Microspheres (F8887) were purchased from Thermo-Fisher Scientific (MA, USA). DAB kit (SK-4100) was obtained from Vector Laboratories (Burlingame, CA, USA). The click chemistry based-Edu kits (C0071S) and Cell Counting Kit-8(C0038) were purchased from Beyotime (Shanghai, China).

Cell culture

Human embryonic kidney cell line HEK293 cell (CRL-1573), human cervical epithelial carcinoma cell line HeLa cell (CCL-2), and murine macrophage cell line RAW264.7 cell (TIB-71) were purchased from the American Type Culture Collection (ATCC). These cell lines were maintained in Dulbecco's modified Eagle's medium (DMEM) supplemented with 10% fetal bovine serum and 1% penicillin-streptomycin. The NSCLC cell lines including NCI-H1975, HCC827, H1299, and A549 were purchased from the ATCC. Primary mouse lung cancer cell line 4347 with overexpressing human EGFR L858R mutation was provided from Dr. Maojin Yao's lab (Guangzhou Medical University, Guangdong). Human T cell line Jurkat was obtained from Dr. Xin Chen's lab (University of Macau, Macau). These cell lines were maintained in 1640 medium (Gibco) supplemented with 10% fetal bovine serum and 1% penicillin-streptomycin. BMDMs were obtained by flushing the femur and tibia from male C57BL/6 mice (8–12 weeks), and the isolated cells were cultured in DMEM medium supplemented with 10% fetal bovine serum (FBS), 20ng/mL M-CSF, and 1% penicillin and streptomycin. The culture medium was changed every 3 days and cells were collected on day 6–7. All cultures were incubated at 37°C in a humidified 5% CO_2 atmosphere, with medium refreshed every 48-72 hours. Cell lines authentication was carried out by mycoplasma detection prior to experimental use.

***In vitro* efferocytosis assay**

For induction of apoptosis, human Jurkat T cells were stained with either pHrodo or celltracker, , resuspended in 1640 medium contained 5% FBS, treated with 150 mJ cm^{-2} ultraviolet C irradiation and incubated for 3-4 h at 37 °C with 5% CO_2. BMDMs were pre-stained with either CFSE or CMFDA and were plated in 96-wells. BMDMs were incubated with apoptotic targets at a 1:5 phagocyte: target ratio for the indicated times. Phagocytosis was assessed by a Live-cell imaging system (Opera Phenix Plus High-Content Screening System). As alternative targets for phagocytosis, BMDMs were incubated with live Jurkat cells or Fluores-Microspheres, at a 1:5 phagocyte: target ratio for the indicated times. When applicable, BMDMs pretreated with peptide/ MacroTAC (0.1-10 μM) for 10 mins, cytochalasin D (10 μM) for 60 mins, competitive peptide (20 μM) for 30 mins, and COL (10 μM) for 3hrs.

ELISA

TGF-β and IL-10 levels were measured in supernatants of BMDMs by using Mouse ELISA Kit (JONLNBIO, Shanghai).

Immunofluorescence staining

For immunofluorescence analysis of cells sample, cells were fixed using 4% paraformaldehyde (PFA) for 30 mins. After fixation, cells were washed with PBS and PBST (PBS contained 0.3% Triton X-100) for 3 times. The cells were then incubated with 5% bovine serum albumin, 0.3% Triton X-100 in PBS for blocking

30mins before incubation in primary antibodies at 4 °C overnight. Samples were washed 3 times with PBS prior to incubation with secondary antibodies for 1 h at room temperature. When observing the colocalization between FITC-MacroTAC, the FITC-MacroTAC(1 μM) was diluted in DMEM and incubated with cells after secondary antibodies incubating for 30 mins. After nuclear staining, the cells were imaged by confocal microscopy.

For immunofluorescence analysis of frozen tissue, mouse tissue (colon and tumor) was embedded in OCT after fixing and denaturization. Tissue blocks were sectioned (10 μm) with a cryostat and mounted on SuperFrost Plus slides. After sectioning, tissue was fixed in 4% PFA for 30 mins. After fixation, tissue was washed with PBS and was blocked in buffer containing 5% bovine serum albumin, 0.3% Triton X-100 in PBS, for 1h at room temperature before incubation in primary antibodies at 4 °C overnight. Samples were washed 3 times with PBS prior to incubation with secondary antibodies for 2 h at room temperature.

Flow cytometry-based peptide-live cell affinity detection

This method has been described by Dr. S.A. Hunter and Dr. J.R. Cochran [25] with minor modification in this study. In brief, the FITC conjugated peptide was diluted with DMEM to different dosages, and co-incubated with live cells in 1.5 mL Eppendorf tubes for 2 hrs at 4 °C. Cells were washed with 0.5 mL of cold PBS containing 1% FBS and analyzed using flow cytometry. The competition experiment followed very similar steps to those listed in the direct-binding assay. The competitive peptide (usually 20 μM) was co-incubated with cells for 30 mins at 4 °C, after that, incubating cells with both the MacroTAC and competitive peptide for 2hrs at 4 °C. Cells were washed with 0.5 mL of cold PBS containing 1% FBS and analyzed using flow cytometry.

DSS-induced mouse colitis model

Male C57BL/6J mice (male, 8-week-old) were administrated with 3.5% DSS-contained drinking water for 5 days, followed by normal drinking water for another 2 days. Body weight, fecal blood, and stool consistency were measured daily. DAI score was defined as follows: weight loss: 0 (no loss), 1 (1–5%), 2 (5–10%), 3 (10–20%), and 4 (> 20%); bleeding: 0 (no blood), 1 (hemoccult positive), 2 (hemoccult positive and visual pellet bleeding), and 4 (gross bleeding); stool consistency: 0 (normal), 2 (loose stool), and 4 (diarrhea). On the day of sacrifice, the colon was collected, and the length was measured. Each colon was divided into 3 parts. A 0.5 cm segment of distal colon was placed into 4% PFA and the remaining two parts were stored at 80°C for further analysis.

Pharmacokinetic and biodistribution studies

Serum stability was assessed *in vitro* by incubating 1 mM peptides with mouse serum at 37°C for various durations [40]. At each time point, ice-cold acetonitrile was added to terminate the reaction, followed by vortexing and standing for 1 min. Deionized water containing 1% trifluoroacetic acid (TFA) was then added, and the

mixture was centrifuged (13,000g, 10 min) to collect the supernatant. The remaining peptide content was analyzed by reverse-phase high-performance liquid chromatography-mass spectrometry (RP-HPLC-MS). Stability was expressed as the percentage of intact peptide remaining relative to the initial amount.

To evaluate tissue distribution and target engagement, DSS-induced colitis was established in mice by administering 3.5% DSS in drinking water for 5 days. On day 5, mice received an intravenous injection of FITC-eMacroTAC or FITC-sc-MacroTAC (5 mg/kg). At 1 h and 6 h post-injection, mice were euthanized, and organs were harvested. Tissues were homogenized in lysis buffer, and fluorescence intensity was measured to quantify peptide accumulation.

Histology

Colon tissue was fixed overnight in 4% PFA, embedded in paraffin, and sectioned into 4-μm-thick slices. Slides were stained separately with HE. The histological score represents the sum of the epithelial damage and inflammatory cell infiltration scores, and these scores were evaluated as described previously [41]. For epithelial damage, the scores were calculated as: 0, normal morphology; 1, loss of goblet cells; 2, loss of crypts; and 4, large areas with crypt loss. For inflammatory cell infiltration, the scores were calculated as: 0, no infiltration; 1, infiltration around crypt bases; 2, infiltration reaching the lamina muscularis mucosae; 3, extensive infiltration reaching the lamina muscularis mucosae and thickening of the mucosa with abundant edema; and 4, infiltration of the lamina submucosa.

Immunoblotting

For protein analysis, cells were washed once with ice-cold phosphate-buffered saline (PBS) and lysed in denaturing buffer (20% glycerol, 2% SDS, 62.5 mM Tris pH 6.8, 2 mM DTT) supplemented with phosphatase inhibitor cocktail and protease inhibitor cocktail on ice. Lysates were boiled at 100°C for 6 min to denature proteins and stored at -80°C until use. Total protein concentration was quantified using a bicinchoninic acid (BCA) assay. Protein samples were mixed with 4×Laemmli Sample Buffer containing 1% 2-mercaptoethanol, denatured at 100°C for 10 min, and run on 12% SDS-polyacrylamide gels under reducing conditions. Separated proteins were electrophoretically transferred to Immun-Blot PVDF membranes using a Trans-Blot Turbo system (Bio-Rad). Membranes were blocked with SuperBlock™ Blocking Buffer for 30 min at room temperature and subsequently incubated overnight at 4°C with primary antibodies diluted in TBST (1× TBS, 0.1% Tween-20) containing 1:1000 antibody solution. After three washes with TBST, membranes were incubated for 1 h at room temperature with horseradish peroxidase (HRP)-conjugated secondary antibodies 1:5000 dilution in TBST. Protein bands were visualized using Clarity Western ECL Substrate and imaged on a ChemiDoc™ Touch Imaging System (Bio-Rad). Band intensities were quantified using Image Lab™ v6.1 software (Bio-Rad).

Cell viability determination

Tumors cells were treated with MacroTAC at different concentration. The cell viability was evaluated by using Cell Counting Kit-8 (CCK-8) with the experimental conditions as the CCK-8 manual.

Stable cell line generation

Lentiviral particles were produced in HEK293T cells via polyethyleneimine (PEI)-mediated co-transfection. For the establishment of EGFR-overexpressing stable cell lines (EGFR-WT), the third-generation packaging plasmids psPAX2 (Addgene, 12260) and pMD2.G (Addgene, 12259) were co-transfected with the target plasmid pLV2-CMV-EGFR(human)-EGFP-Puro (Miaoling, P62502). For the establishment of EGFR-knockdown stable cell lines (EGFR-KD), the packaging plasmids psPAX2 and pMD2.G were co-transfected with the EGFR-shRNA lentiviral plasmid pLVX-U6-EGFR-shRNA-puro (the target sequences shRNA1: AGAATGTGGAATACCTAAGG; shRNA2: GCCACAAAGCAGTGAATTTAT). Viral supernatants were collected at 48 hours post-transfection, pooled, and concentrated by centrifugation at 2,000 g for 10 minutes. The concentrated viral supernatants were then sterilized by filtration through a 0.22 μm sterile filter. NCI-H1975 and HCC827 cells were used as recipient cells for EGFR-KD experiments, while EGFR-KD HCC827 cells were used as recipient cells for EGFR-WT experiments. The respective recipient NSCLC cell lines were transduced with the concentrated lentiviral particles and selected with 10 μg/mL puromycin for 7-14 days to obtain stable polyclonal cell populations. The stable integration of the target genes (EGFR overexpression or knockdown) was verified by western blot analysis to detect the expression level of EGFR protein.

Single-cell RNA Sequencing Data Analysis

Raw sequencing data were processed using CellRanger [42] (v8.0) with the Count pipeline to align reads to the mouse reference genome (mm10). The resulting gene-by-cell unique molecular identifier (UMI) count matrix was analyzed using the R package Seurat [43] (v5.0). Quality control was first applied to remove low-quality barcodes: cells with fewer than 200 detected genes (potential debris) and more than 8,000 genes (potential doublets or high-viability artifacts) and those with > 5% mitochondrial gene expression (potential apoptotic cells) were excluded. Subsequently, doublets were further identified and removed using DoubletFinder [44] (v2.0.6). Following cell filtering, raw UMI counts were log-normalized and scaled. Highly variable features were selected, and linear dimensionality reduction was performed via principal component analysis (PCA). Batch effects across samples were corrected by applying Harmony [45] (v1.2.4) to the PCA embeddings. Cellular clusters were resolved by applying the Louvain algorithm (resolution = 0.5) to a K-nearest neighbor (KNN) graph constructed on the corrected PCA space. For visualization, both Uniform Manifold Approximation and Projection (UMAP) and t-distributed stochastic neighbor embedding (t-SNE) were used. Cell type identities were assigned by performing differential gene

expression analysis (Wilcoxon rank-sum test) for each cluster and annotating based on canonical marker genes. Cell type proportions across experimental conditions were calculated and statistically compared using scProportionTest [46] (v0.0.0.9) with 10,000 permutations. *P*-values were adjusted for multiple testing using the Benjamini–Hochberg procedure.

Macrophage Subset Re-clustering and Characterization

Macrophage populations were extracted from the integrated dataset for subset analysis. Re-normalization, variable feature selection, scaling, and PCA were performed on macrophage cells. Sub-clustering was conducted following the same workflow with optimized resolution 0.2, identifying 3 distinct macrophage subtypes. Following initial clustering, subtype-specific differentially expressed genes (DEGs) were identified with FindAllMarkers function from Seurat (v5.0). The biological functions of these subtypes were then interrogated by performing Gene Ontology (GO) enrichment analysis (Biological Process domain) on the upregulated DEGs using the enrichGO tool within the clusterProfiler [47] (v.4.18.1) framework. Proportions of macrophage subsets across treatment groups were compared using the same statistical approach described above.

Mrc1-stratified Gene Set Enrichment Analysis

Macrophages were stratified into Mrc1-positive (Mrc1+) and Mrc1-negative (Mrc1−) populations based on normalized gene expression (threshold: normalized expression > 0). For each Mrc1 subgroup, differential gene expression analysis was performed between treatment conditions using the Wilcoxon rank-sum test. Genes with adjusted p-value < 0.05 and |log2FC| > 0.25 were considered differentially expressed.

Pre-ranked Gene Set Enrichment Analysis (GSEA) was conducted separately for Mrc1+ and Mrc1− macrophage populations using clusterProfiler6 (v. 4.18.1). Gene Ontology Biological Process (GO BP) gene sets were obtained from org.Mm.eg.db, version 3.22.0. GSEA parameters included minimum gene set size of 15, maximum of 500, and 1000 permutations. Pathways with adjusted p-value < 0.05 and |NES| > 1 were considered significantly enriched.

Cell Density Analysis of Macrophage subpopulations

To assess cellular abundance shifts between disease and peptide treatment within the UMAP embedding, two-dimensional kernel density estimation was applied to the UMAP coordinates of cells from each experimental group using the kde2d function (MASS v.7.3-65) with a Gaussian kernel. The resulting density surfaces were normalized to a [0,1] scale to ensure cross-group comparability and visualized as heatmaps overlaid on UMAP projections.

Efferocytosis Module Score Analysis

10 Efferocytosis-related genes, including Mertk, Gas6, Mfge8, C1qa, Itgav, Elmo1, Rac1, Pparg, Abca1, Il10, were obtained from the Kyoto Encyclopedia of Genes and

Genomes (KEGG) database [48] (pathway: mmu04148). Efferocytosis module scores were calculated for each cell using the AddModuleScore function in Seurat (v5.0), which computes the average expression of signature genes relative to control gene sets randomly selected from genes with similar expression levels. Module scores were compared across macrophage subsets, treatment groups, and Mrc1+/Mrc1− populations using the Wilcoxon rank-sum test. P-values were adjusted using the Benjamini-Hochberg method.

Tumor xenograft model

The anti-tumor efficacy of tMacroTAC was evaluated in an HCC827 xenograft model. Male nude mice (4–6 weeks old) were subcutaneously inoculated with 5 × 10^6 HCC827 cells in 100 µL PBS mixed with Matrigel (1:1) into the right flank. When tumors reached approximately 100 mm^3, mice were randomly assigned to the indicated treatment groups. tMacroTAC (1 mg/kg) was administered by intratumoral injection every 2–3 days. Anti-CD47 blocking antibody (B6H12, 200 µg per mouse) was administered by intraperitoneal injection every 2–3 days. For competitive inhibition experiments, CD206-targeting peptide (CD206pep, 5 mg/kg) was co-administered *i.p.* with tMacroTAC. Tumor volumes were measured every 2 days using a caliper and calculated using the formula: volume = (length × $width^2$)/2. Mice were monitored for body weight changes throughout the treatment period as an indicator of systemic toxicity. At the end of the experiment, mice were euthanized, and tumors were excised, photographed, and weighed for further analysis.

Proliferation assay

The anti-proliferative effect of tMacroTAC was evaluated using EdU incorporation, CFSE dilution, and clonogenic formation assays. During these experiments, the tumor cells were cultured with low serum medium (1% FBS).

For EdU assay, tumor cells were seeded in 96-well plates overnight, followed by stimulation with EGF (30 ng/mL) in the presence or absence of tMacroTAC at indicated concentrations for 24 h. EdU (5-ethynyl-2'-deoxyuridine) was added during the final 2 h of culture, and cells were processed according to the manufacturer‘s protocol (Click EdU Kit, Beyotime). Nuclei were counterstained with Hoechst 33342. EdU-positive cells were quantified using the Opera Phenix Plus High-Content Screening System.

For CFSE dilution assay, cells were labeled with 5 µM CFSE for 10 min at 37°C, washed, and then cultured with EGF (30 ng/mL) in the presence or absence of tMacroTAC at indicated concentrations. After 72 h, cells were harvested, and CFSE fluorescence was analyzed by flow cytometry. Proliferation was quantified as the percentage of cells with diluted CFSE signal.

For clonogenic formation assay, cells were seeded in 6-well plates at low density (500 cells per well) and cultured with EGF (30 ng/mL) in the presence or absence of tMacroTAC for 7–10 days. Colonies were fixed with 4% PFA, stained with 0.1% crystal violet, and imaged by an iPhone (Apple Inc.).

Statistical analysis

Data are presented as mean ± SD unless otherwise indicated. For animal experiments involving body weight and disease activity index (DAI) over time, data are presented as mean ± SEM. Statistical analyses were performed using GraphPad Prism or R. For two-group comparisons, unpaired two-tailed Student's t-test was used. For multiple-group comparisons, one-way ANOVA was performed. For single-cell RNA-seq data, two-group comparison was assessed using Mann-Whitney U test, multi-group comparison was using Wilcoxon rank-sum test.

Competing interests

The authors declare no competing interests.

ACKNOWLEDGMENTS

This study was supported by Science and Technology Development Fund, Macau SAR (FDCT) (File no. 0040/2024/RIB1, 0025/2022/A1, 0002/2025/NRP), the National Natural Science Foundation of China(NSFC) (No. 82271455), and the University of Macau grants (File no. MYRG-GRG2024-00238-ICMS-UMDF, MYRG-GRG2023-00089-ICMS-UMDF) awarded to Jia-Hong Lu, the National Natural Science Foundation of China (No. 825B200100) to Zhengyu Ren, and FDCT fund(0040/2025/ITP1), joint FDCT-NSFC fund (0145/2025/AFJ) and UM MYRG-GRG2024-00272-FHS to Chen MING. We thank Prof. Jinjian Lu and Dr. Zihan Ye (University of Macau) for help with the tMacroTAC mediated tumor cell phagocytosis assay. We also thank Prof. Xianxing Jiang and Ms. Can Xiao (Sun Yat-Sen University) for the support of the protocol about serum peptide stability experiment. This study was done with technical help from the Institute of Chinese Medical Sciences and Faculty of Health Sciences at University of Macau.

AUTHOR CONTRIBUTIONS

JH.L. conceived and supervised the project; ZY.R. designed and conducted the experiments, acquired and analyzed the data, and drafted the manuscript; C.M. and JX.Y. contributed to the analysis of scRNAseq data; XZ.G. contributed to the construction of transgenic tumor cell line and corresponding validation; JT.L. contributed to the detection and validation of MacroTAC-targets binding affinity; ZK.Z. contributed to the pKa analysis; JR.S., TY.C., YS.J. and WW.D. contributed to the validation of pro-efferocytotic function of MacroTAC and animal experiments; MY.W., YT.W., XX.Z., R.H. and EJ.W. contributed to the project discussion and optimization; M.L. contributed to the validation of MacroTAC-targets binding affinity; M.L., MJ.Y., Y.Z. and JY.R. contributed to the animal experiments and project discussion.

Reference

1. Sakamoto, K.M., et al., Protacs: chimeric molecules that target proteins to the Skp1-Cullin-F box complex for ubiquitination and degradation. Proc Natl Acad Sci U S A, 2001. 98(15): p. 8554-9.
2. Bekes, M., D.R. Langley, and C.M. Crews, PROTAC targeted protein degraders: the past is prologue. Nat Rev Drug Discov, 2022. 21(3): p. 181-200.
3. Campone, M., et al., Vepdegestrant, a PROTAC Estrogen Receptor Degrader, in Advanced Breast Cancer. N Engl J Med, 2025. 393(6): p. 556-568.
4. Banik, S.M., et al., Lysosome-targeting chimaeras for degradation of extracellular proteins. Nature, 2020. 584(7820): p. 291-297.
5. Li, Z., et al., Allele-selective lowering of mutant HTT protein by HTT-LC3 linker compounds. Nature, 2019. 575(7781): p. 203-209.
6. Fu, Y., et al., Degradation of lipid droplets by chimeric autophagy-tethering compounds. Cell Res, 2021. 31(9): p. 965-979.
7. Tan, S., et al., Targeted clearance of mitochondria by an autophagy-tethering compound (ATTEC) and its potential therapeutic effects. Sci Bull (Beijing), 2023. 68(23): p. 3013-3026.
8. Jung, H., et al., Anti-inflammatory clearance of amyloid-beta by a chimeric Gas6 fusion protein. Nat Med, 2022. 28(9): p. 1802-1812.
9. Morioka, S., et al., Chimeric efferocytic receptors improve apoptotic cell clearance and alleviate inflammation. Cell, 2022. 185(26): p. 4887-4903 e17.
10. Willingham, S.B., et al., The CD47-signal regulatory protein alpha (SIRPa) interaction is a therapeutic target for human solid tumors. Proc Natl Acad Sci U S A, 2012. 109(17): p. 6662-7.
11. Majeti, R., et al., CD47 is an adverse prognostic factor and therapeutic antibody target on human acute myeloid leukemia stem cells. Cell, 2009. 138(2): p. 286-99.
12. Tseng, D., et al., Anti-CD47 antibody-mediated phagocytosis of cancer by macrophages primes an effective antitumor T-cell response. Proc Natl Acad Sci U S A, 2013. 110(27): p. 11103-8.
13. Scodeller, P., et al., Precision Targeting of Tumor Macrophages with a CD206 Binding Peptide. Sci Rep, 2017. 7(1): p. 14655.
14. Asciutto, E.K., et al., Phage-Display-Derived Peptide Binds to Human CD206 and Modeling Reveals a New Binding Site on the Receptor. J Phys Chem B, 2019. 123(9): p. 1973-1982.
15. Lepland, A., et al., Targeting Pro-Tumoral Macrophages in Early Primary and Metastatic Breast Tumors with the CD206-Binding mUNO Peptide. Mol Pharm, 2020. 17(7): p. 2518-2531.
16. Lepland, A., et al., Peptide-Drug Conjugate for Therapeutic Reprogramming of Tumor-Associated Macrophages in Breast Cancer. Adv Sci (Weinh), 2025. 12(10): p. e2410288.
17. Park, S., et al., TLR4/MD2 specific peptides stalled in vivo LPS-induced immune exacerbation. Biomaterials, 2017. 126: p. 49-60.
18. Houimel, M. and L. Mazzucchelli, Random phage-epitope library based identification of a peptide antagonist of Mac-1 beta2 integrin ligand binding. Matrix Biol, 2012. 31(1): p. 66-77.
19. Berntzen, G., et al., Characterization of an FcgammaRI-binding peptide selected by phage display. Protein Eng Des Sel, 2006. 19(3): p. 121-8.
20. Cieslewicz, M., et al., Targeted delivery of proapoptotic peptides to tumor-associated

macrophages improves survival. Proc Natl Acad Sci U S A, 2013. 110(40): p. 15919-24.

21. Xiong, C., et al., Peptide-based imaging agents targeting phosphatidylserine for the detection of apoptosis. J Med Chem, 2011. 54(6): p. 1825-35.
22. Guan, S., et al., Phosphatidylserine targeting peptide-functionalized pH sensitive mixed micelles for enhanced anti-tumor drug delivery. Eur J Pharm Biopharm, 2020. 147: p. 87-101.
23. Rojiani, M.V., et al., In vitro interaction of a polypeptide homologous to human Ro/SS-A antigen (calreticulin) with a highly conserved amino acid sequence in the cytoplasmic domain of integrin alpha subunits. Biochemistry, 1991. 30(41): p. 9859-66.
24. Kim, D.Y., et al., Imaging Calreticulin for Early Detection of Immunogenic Cell Death During Anticancer Treatment. J Nucl Med, 2021. 62(7): p. 956-960.
25. Hunter, S.A. and J.R. Cochran, Cell-Binding Assays for Determining the Affinity of Protein-Protein Interactions: Technologies and Considerations. Methods Enzymol, 2016. 580: p. 21-44.
26. Wu, M.Y., et al., PI3KC3 complex subunit NRBF2 is required for apoptotic cell clearance to restrict intestinal inflammation. Autophagy, 2021. 17(5): p. 1096-1111.
27. Morioka, S., C. Maueroder, and K.S. Ravichandran, Living on the Edge: Efferocytosis at the Interface of Homeostasis and Pathology. Immunity, 2019. 50(5): p. 1149-1162.
28. Mehrotra, P. and K.S. Ravichandran, Drugging the efferocytosis process: concepts and opportunities. Nat Rev Drug Discov, 2022. 21(8): p. 601-620.
29. Maschalidi, S., et al., Targeting SLC7A11 improves efferocytosis by dendritic cells and wound healing in diabetes. Nature, 2022. 606(7915): p. 776-784.
30. Lee, C.S., et al., Boosting Apoptotic Cell Clearance by Colonic Epithelial Cells Attenuates Inflammation In Vivo. Immunity, 2016. 44(4): p. 807-20.
31. Wu, M.Y., et al., Enhancement of LC3-associated efferocytosis for the alleviation of intestinal inflammation. Autophagy, 2024: p. 1-2.
32. Wu, M.Y., et al., Enhancement of efferocytosis through biased FPR2 signaling attenuates intestinal inflammation. EMBO Mol Med, 2023. 15(12): p. e17815.
33. Li, Z., et al., Identification and characterization of a novel peptide ligand of epidermal growth factor receptor for targeted delivery of therapeutics. FASEB J, 2005. 19(14): p. 1978-85.
34. Gresham, H.D., et al., A novel member of the integrin receptor family mediates Arg-Gly-Asp-stimulated neutrophil phagocytosis. J Cell Biol, 1989. 108(5): p. 1935-43.
35. Jin, R., L. Neufeld, and T.L. McGaha, Linking macrophage metabolism to function in the tumor microenvironment. Nat Cancer, 2025. 6(2): p. 239-252.
36. Sordella, R., et al., Gefitinib-sensitizing EGFR mutations in lung cancer activate anti-apoptotic pathways. Science, 2004. 305(5687): p. 1163-7.
37. Grant, S., L. Qiao, and P. Dent, Roles of ERBB family receptor tyrosine kinases, and downstream signaling pathways, in the control of cell growth and survival. Front Biosci, 2002. 7: p. d376-89.
38. Mariko Morimoto, D.S.R., Ru Wen, Ell Handy, Eric E. Peterson, Grace M. Stepek, Nicholas A. Till, James D. Brooks, Carolyn R. Bertozzi., Tumor Immune Cell Targeting Chimeras (TICTACs) reprogram tumor-associated macrophages. BioRxiv, 2023.
39. Du, M., et al., Chimeras co-targeting antigens and FcgammaRIIb trigger degradation of

extracellular soluble proteins and pathological aggregates. Nat Commun, 2025. 17(1): p. 514.

40. Song, N., et al., Design and Discovery of Novel Cyclic Peptides as EDPs-EBP Interaction Inhibitors for the Treatment of Liver Fibrosis. J Med Chem, 2023. 66(7): p. 4689-4702.
41. Kim, J.J., et al., Investigating intestinal inflammation in DSS-induced model of IBD. J Vis Exp, 2012(60).
42. Zheng, G.X., et al., Massively parallel digital transcriptional profiling of single cells. Nat Commun, 2017. 8: p. 14049.
43. Hao, Y., et al., Dictionary learning for integrative, multimodal and scalable single-cell analysis. Nat Biotechnol, 2024. 42(2): p. 293-304.
44. McGinnis, C.S., L.M. Murrow, and Z.J. Gartner, DoubletFinder: Doublet Detection in Single-Cell RNA Sequencing Data Using Artificial Nearest Neighbors. Cell Syst, 2019. 8(4): p. 329-337 e4.
45. Korsunsky, I., et al., Fast, sensitive and accurate integration of single-cell data with Harmony. Nat Methods, 2019. 16(12): p. 1289-1296.
46. Miller, S.A., et al., LSD1 and Aberrant DNA Methylation Mediate Persistence of Enteroendocrine Progenitors That Support BRAF-Mutant Colorectal Cancer. Cancer Res, 2021. 81(14): p. 3791-3805.
47. Wu, T., et al., clusterProfiler 4.0: A universal enrichment tool for interpreting omics data. Innovation (Camb), 2021. 2(3): p. 100141.
48. Kanehisa, M. and S. Goto, KEGG: kyoto encyclopedia of genes and genomes. Nucleic Acids Res, 2000. 28(1): p. 27-30.

Figure 1 | Design, screening, and functional characterization of the efferocytosis-targeting MacroTAC (effero-MacroTAC).
a, Schematic illustration of the effero-MacroTAC concept: a bifunctional peptide chimera bridges targeted proteins express on macrophages and apoptotic cells (ACs) to enhance efferocytosis. **b**, Strategy for constructing and screening the effero-MacroTAC peptide library. Five macrophage-targeting peptides and two AC-targeting peptides were combinatorially conjugated via a GSGS linker to generate ten unique bispecific candidates for screening. **c, d**, Representative images and quantification of screening data for 10 candidate chimeras in the efferocytotic binding assay. The CD206-CRT chimera was selected as the lead. Peptide dosage, 1μM. **e**, Affinity of eMacroTAC binding to purified mouse CD206 protein (left) and human calreticulin protein (right) by Microscale Thermophoresis (MST) assay. **f**, Representative images and quantification of eMacroTAC induced ACs uptake with or without PS blockade by Annexin V. eMacroTAC, 1μM. **g**, Quantification of eMacroTAC induced ACs binding to BMDMs with or without internalization blocking by Cytochalasin D (10μM). eMacroTAC, 1μM. **h**, Quantification of efferocytosis assay comparing the active eMacroTAC to sc-MacroTAC. **j**, Elisa assay of TGF-β in the supernatant of BMDMs following efferocytosis in the presence or absence of eMacroTAC. eMacroTAC and sc-MacroTAC, 1μM.

Figure 2 | Cellular binding specificity and receptor engagement of effero-MacroTAC.
a, Design of FITC-eMacroTAC and FITC-sc-MacroTAC. **b, c,** Representative images (b) and quantification (c) of FITC-eMacroTAC binding to fixed BMDMs. **d-g,** Representative images (e) and quantification (f) of FITC-eMacroTAC binding to fixed apoptotic Jurkat cells, and flow cytometry histograms of apoptosis-dependent binding of FITC-eMacroTAC (g). **h,** Representative images of FITC-eMacroTAC binding to live BMDMs. **i,** Direct cell-surface binding affinity of eMacroTAC for live BMDMs, determined by flow cytometry. Kd is indicated. **j,** Design of Cy5-labeled mannose (Cy5- mannose) induced eMacroTAC endocytosis experiment. **k,** Representative images of FITC-eMacroTAC binding to live BMDMs with or without Cy5-mannose treatment at indicated time points. The dosage of FITC-eMacroTAC and FITC-sc-MacroTAC used in this Figure is 10μM.

Figure 3| Effero-MacroTAC alleviates DSS-induced colitis *in vivo*.
a, b, Representative immunofluorescence images (a) and quantification (b) of $CD206^+$ macrophage infiltration in the colon during DSS-induced colitis; n=4-5 mice per group. **c-e,** Mice were administered 3.5% DSS in drinking water for 5 days, accompanied by daily intravenous injections of eMacroTAC (1mg/kg) or PBS, sc-MacroTAC (1mg/kg) with or without a competitive CD206 blocking peptide (5mg/kg) for 7 days. Body weight change (c), disease activity index (d) and colon length (e) of mice were measured; n=9 mice per group. **f-i**, Representative images of H&E staining (f) and TUNEL staining (g) and their quantification (h, i) in colon sections.

Figure 4 | Single-cell RNA sequencing reveals colitis alleviation, and identifies specific CD206$^+$ macrophage efferocytosis enhancement and reprogramming in the treatment of DSS induced colitis.

a, UMAP plot of cells from colonic tissues from mice induced with DSS, illustrating 13 different cell types including 3 macrophage subsets. **b,** Dot plot of GO enrichment analysis defining the functional divergence among 3 macrophage subsets. **c,** Compositional changes of the overall cell types after eMacroTAC treatment. **d,** Proportional changes of macrophage subsets upon eMacroTAC treatment. **e,** Violin plots showing expression changes of key functional genes in macrophage subsets. **f, g,** Gene Set Enrichment Analysis (GSEA) of efferocytosis-related pathways in Mrc1+ (f) and Mrc1- (g) macrophages from eMacroTAC-treated mice. **h,** Module scoring analysis demonstrates preferential activation of the efferocytosis pathway in Mrc1+ (f) macrophages after eMacroTAC-treatment. **i,** Violin plots of efferocytosis-related genes demonstrate divergent transcriptional responses to DSS and eMacroTAC treatment between Mrc1$^+$ (f) and Mrc1$^-$ (g) macrophages. n=3 mice per group.

Figure 5 | Genetic ablation of MerTK abolishes anti-colitis function of MacroTAC *in vivo*.

a, Flow cytometry access of MerTK surface expression using BMDMs from WT and MerTK-KO mice. **b,** Quantification of efferocytosis assay in BMDMs from of WT and MerTK-KO mice with or without eMacroTAC (1μM) treatment. **c,** Schematic of the *in vivo* colitis experiment in WT and MerTK-deficient mice. **d-g**, Therapeutic effects of eMacroTAC (1mg/kg) in WT and MerTK-deficient mice: body weight change (d), disease activity index (e), colon length (f, g). **h, i,** Representative images (h) and quantification of histological score (i) from the H&E-stained colon sections from WT and MerTK-deficient mice with or without eMacroTAC treatment. n=8 per group for WT; n=5-6 per group for MerTK KO.

Figure 6 | Design and validation of tumor-MacroTAC.

a, b, Schematic illustration of the tumor-MacroTAC concept: a bifunctional peptide chimera bridges tumor-associated macrophages (TAMs) and EGFR expressing tumor cells to enhance phagocytosis through interacting with CD206 and EGFR. **c, g,** Binding affinity of tMacroTAC for recombinant CD206 (c) and EGFR (g) proteins detected by MST. Kd is indicated. **d, h,** Live cell binding affinity of FITC-tMacroTAC binding to live BMDMs (d) and live HCC827 cells (h) detected by cytometry. **e,** Representative images of FITC-tMacroTAC (1μM) binding to live BMDMs. **i,** Representative images of FITC-tMacroTAC (10μM) co-localized with EGFR protein in HCC827 cell line. **f,** Western blot of EGFR expression in different cell lines. **j,** Cytometry based phagocytotic assay of tMacroTAC (1μM) enhanced phagocytosis of HCC827 cells by BMDMs in the presence of anti-CD47 antibody B6H12 (3.1μg/mL). **k,** Representative images of internalized tumor cell co-localized with the lysosome of BMDMs stained with lysotracker. **l,** Competitive

inhibition of phagocytosis enhancement by free CD206-targeting peptide. tMacroTAC, 1μM; CD206pep, 20μM; B6H12, 3.1μg/mL. **m-o,** EGFR-dependence of phagocytosis: effect on EGFR-knockdown HCC827 cells (m), upon re-expression of WT-EGFR (n), and in EGFR-knockdown NCI-H1975 cells (o). tMacroTAC, 1μM; B6H12, 3.1μg/mL.

Figure 7 | Tumor-MacroTAC inhibits HCC827 tumor growth *in vivo* via combined mechanisms.

a, Schematic of the *in vivo* tMacroTAC therapeutic experiment of HCC827 xenograft model. B6H12, 200μg/kg; tMacroTAC, 1mg/kg; CD206pep, 5mg/kg. n=8 mice per group. **b,** Tumor growth curves under different treatments. The corresponding treatment is indicated. **c,** Representative photographs of excised tumors. **d, e,** Representative immunohistochemical staining for cleaved caspase-3 (d) and immunofluorescence staining for Ki67 (e) in tumor sections. **f, g,** Quantification of cleaved caspase-3^+ area (f) and $Ki67^+$ tumor cells (g). **h, i,** *In vitro* anti-proliferative effects on HCC827 cells by tMacroTAC: EdU assay (h) and CFSE dilution assay (i).

Extended Data Figure 1 | Development, screening, and validation of Effero-MacroTAC.

a, Schematic workflow of the *in vitro* efferocytosis assay using BMDMs and UV-induced apoptotic cells (ACs). **b-d** Representative cytometry graphs of surface expression of CD206 (b), CD16/32 (c), and CD11b (d) on BMDMs with or without IL-4 induction. **e,** Representative cytometry graphs of surface expression of PS and calreticulin on Jurkat cells with or without UV induction. **f,** Representative images from all ten candidate eMacroTACs from the primary screen for ACs binding (celltraker-deepred). **g,** Quantification of all ten candidate eMacroTACs from the primary screen for ACs internalization/degradation (pHrodo signal). Columbamine (COL, 10μM) was used as a positive control. **h,** Representative images of dose-response of the eMacroTAC in efferocytosis assay.

i, Competition assay using CD206-binding motif peptide (20μM) and CRT-binding motif peptide(20μM) on eMacroTAC (1μM) mediated efferocytosis. **j,** Representative images (left) and quantification (right) of ACs processing ability of BMDMs with or without eMacroTAC treatment (1μM). **k**, Elisa assay of IL-10 in the supernatant of BMDMs following efferocytosis in the presence or absence of eMacroTAC (1μM).

Extended Data Figure 2 | Validation and charaterization of Effero-MacroTAC.

a, b, Representative images and quantification of fluorescent microsphere (a) and ACs (b) uptake by BMDMs treated with or without eMacroTAC (1μM). **c,** Representative images of live cell (Jurkat) uptake by BMDMs treated with or without eMacroTAC (1μM). **d,** Representative images and quantification of lysosomal intensity in BMDMs using lysotracker red, with or without eMacroTAC

(1μM) treatment. Bafilomycin A1 (BAF A1, 500nM) is used as a negative control, Torin 1 (100nM) is used as a positive control. **e,** Flow cytometry histograms of mannose uptake by BMDMs with or without eMacroTAC (10μM) treatment.

Extended Data Figure 3 | Transcriptomic analysis of effero-MacroTAC-treated macrophages *in vitro* reveals upregulated pro-resolving and downregulated inflammatory pathways post-efferocytosis.
a, Schematic workflow of RNA-seq from BMDMs with or without eMacroTAC treatment. **b,** Pie chart of differentially expressed genes among groups. **c,** Selected enriched pathway by Gene Set Enrichment Analysis (GSEA) showing upregulated pro-resolving and downregulated inflammatory pathways.

Extended Data Figure 4 | Pharmacokinetics and biodistribution of effero-MacroTAC in mice.
a, Plasma concentration-time curve following intravenous injection of eMacroTAC or sc-MacroTAC on wildtype mice. n=3 mice per time point. **b,** Plasma stability analysis of eMacroTAC under physiological conditions. **c, d,** Biodistribution of eMacroTAC in different organs including colon, lung, liver, and spleen at 1 hour (c) and 6 hours (d) on colitis mice. n=3 mice per group. **e,** Representative images and quantification of $CD206^{+}$ macrophages cells colocalizing FITC labeled eMacroTAC (10mg/kg) or sc-MacroTAC (10mg/kg).

Extended Data Figure 5 | Intraperitoneal administration (i.p.) of Effero-MacroTAC alleviates DSS induced-colitis independent of dosage.
a, Schematic of the *in vivo* eMacroTAC therapeutic experiment of DSS induced colitis model via *i.p.* administration at the dosage of 1mg/kg and 5 mg/kg. **b, c**, Therapeutic outcomes measured by body weight change (b), disease activity index (c). **d-g**, Representative images of colon length (d) and H&E staining of colon sections (f) and their quantification (e, g).

Extended Data Figure 6 | Detailed single-cell RNA sequencing analyses.
a, Relative proportions of major annotated cell types, including three macrophage subtypes, across individual samples, shown separately for each cell population. **b, c,** Density projection of macrophages on the UMAP embedding in PBS and eMacroTAC-treated colitis mice. Density was normalized to range [0,1]. White lines indicate regions of equal cell density. **d,** Violin plots showing expression of efferocytosis related genes.

Extended Data Figure 7 | Binding and phagocytosis assays for tumor-MacroTAC.
a, Competitive inhibition of FITC-tMacroTAC (1μM) binding to live BMDMs by anti-CD206 antibody or CD206 binding peptide motif (20μM) detected by flow cytometry. **b,** Surface binding affinity of tMacroTAC to live A549 cells detected by flow cytometry. **c,** FITC-tMacroTAC (10μM) binding to live NCI-H1975 cells with or without EGFR-knockdown. **d,** Representative images of macrophages

phagocytosis of NCI-H1975 tumor cells assay in the prevalence of CD47 antibody B6H12 (3.1μg/mL) with or without tMacroTAC (1μM) treatment. **e,** Gating strategy for the flow cytometry-based phagocytosis assay. **f, g,** Time-lapse images of macrophages phagocytosis of NCI-H1975 cells including internalization and lysosomal digestion. Zoom-in images are indicated as g. B6H12, 3.1μg/mL; tMacroTAC, 1μM.

Extended Data Figure 8 | Tumor-MacroTAC promotes BMDMs phagocytosis of EGFR-variant cell lines.

a-d, Representative cytometry graphs and quantification of macrophages phagocytosis of EGFR expressing A549 (a) and NCI-H1975 (c) cells with or without tMacroTAC treatment. Representative images of colocalization of phagocytosed tumor cells and macrophages' lysosome in the prevalence of anti-CD47 antibody B6H12 (b, d). B6H12, 3.1μg/mL; tMacroTAC, 1μM. **e,** Representative images of co-culturing BMDMs and tumor cells without B6H12. **f,** Quantification of macrophages phagocytosis of EGFR non-expressing Jurkat cells. B6H12, 3.1μg/mL; tMacroTAC, 1μM. **g,** Total EGFR expression and surface EGFR expression of HCC827 cells with or without EGFR knockdown detected by western blot (top) and flow cytometry (bottom). **h**, Representative cytometry graphs of phagocytosis quantifying data corresponding to Fig. 6o. **i,** Surface EGFR expression on HCC827 cells: control, following EGFR knockdown, and after reconstitution of EGFR expression. **j,** Total EGFR expression and surface EGFR expression of NCI-H1975 cells with or without EGFR knockdown detected by western blot (left) and flow cytometry (right).

Extended Data Figure 9 | Characterization of treatment effects and immune regulation by tumor-MacroTAC.

a, H&E staining of the liver and kidney sections from mice receiving the indicated treatments. **b,** Body weight changes of mice during the treatment period. **c,** Representative immunofluorescence images revealed spatial association between Ly6G+ neutrophils and Cleaved caspase-3+ dead cells in tumor sections. **d, e,** Representative immunofluorescence images of Ly6G+ neutrophil infiltration in tumor sections (d) and quantification of neutrophil infiltration (e). **f, g,** Representative immunofluorescence images of chemokine MCP-3 (CCL7) in tumor sections (f) and its colocalization (g). **h, i,** Flow cytometry analysis of CD86 and CD206 expression in IL-4-treated bone marrow-derived macrophages (BMDMs) *in vitro*. **j,** Representative images of BMDMs co-cultured with HCC827 cells in the absence of the anti-CD47 blocking antibody B6H12 at the indicated time points. tMacroTAC, 1μM. **k,** CCK8 assay of HCC827 cell line treated with different dosage of tMacroTAC.

Extended Data Figure 10 | Tumor-MacroTAC inhibits proliferation of EGFR harboring tumor cells in an EGFR mutation dependent manner.

a, Model of tMacroTAC inhibited EGF induced tumor cells via competitively

binding EGFR. **b,** Clonogenic formation assay of HCC827 cell line treated with different dosage of tMacroTAC. EGF, 30ng/mL; tMacroTAC 1μM and 10μM. **c, d,** Representative images from Edu assays in EGFR-knockdown HCC827 cells (c) and upon WT-EGFR re-expression (d), and corresponding quantification. **e, f,** Clonogenic formation assays on corresponding HCC827 cell models. EGF, 30ng/mL; tMacroTAC 1μM and 10μM. **g, h,** EdU assay and quantification in an EGFR-L858R-overexpressing primary mouse lung cancer cell line (g) and in the endogenously L858R-mutant NCI-H1975 cell line (h). EGF, 30ng/mL; tMacroTAC 1μM and 10μM. **i, j,** EdU assay and quantification in EGFR-knockdown NCI-H1975 cells (i) and in wild-type EGFR H1299 cells (j). EGF, 30ng/mL; tMacroTAC 1μM and 10μM.

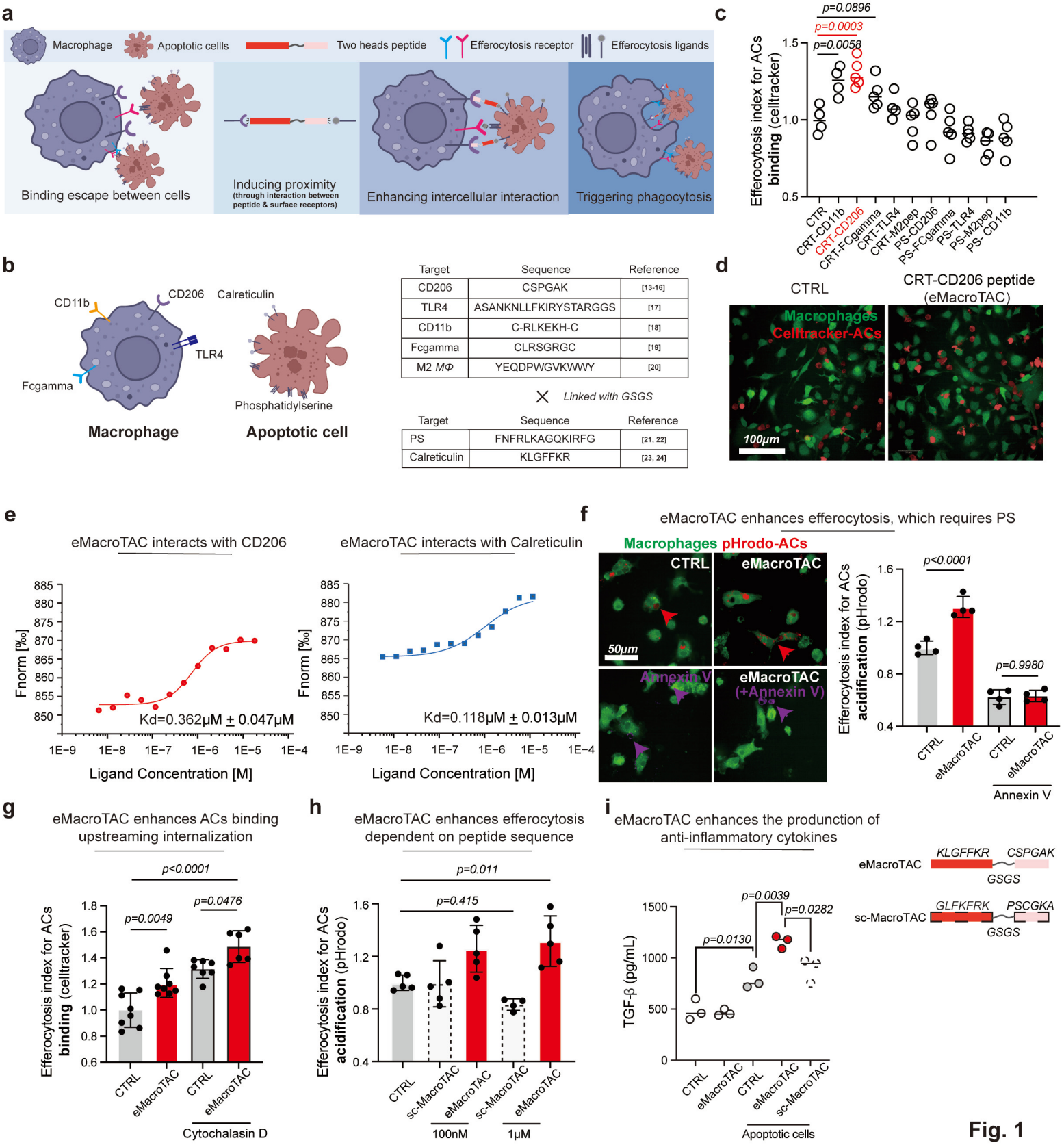
a
Macrophage
Apoptotic cells
Two heads peptide
Efferocytosis receptor
Efferocytosis ligands
Binding escape between cells
Inducing proximity
(through interaction between peptide & surface receptors)
Enhancing intercellular interaction
Triggering phagocytosis
c
p=0.0896
p=0.0003
p=0.0058
Efferocytosis index for ACs binding (celltracker)
CTR
CRT-CD11b
CRT-CD206
CRT-FCgamma
CRT-TLR4
CRT-M2pep
PS-CD206
PS-FCgamma
PS-TLR4
PS-M2pep
PS- CD11b
b
CD11b
CD206
Calreticulin
TLR4
Fcgamma
Phosphatidylserine
Macrophage
Apoptotic cell
Target | Sequence | Reference
CD206 | CSPGAK | [13-16]
TLR4 | ASANKNLLFKIRYSTARGGS | [17]
CD11b | C-RLKEKH-C | [18]
Fcgamma | CLRSGRGC | [19]
M2 MΦ | YEQDPWGVKWWY | [20]
Linked with GSGS
Target | Sequence | Reference
PS | FNFRLKAGQKIRFG | [21, 22]
Calreticulin | KLGFFKR | [23, 24]
d
CTRL
CRT-CD206 peptide (eMacroTAC)
Macrophages
Celltracker-ACs
100µm
e
eMacroTAC interacts with CD206
eMacroTAC interacts with Calreticulin
Fnorm [‰]
Kd=0.362µM ± 0.047µM
Kd=0.118µM ± 0.013µM
Ligand Concentration [M]
f
eMacroTAC enhances efferocytosis, which requires PS
Macrophages pHrodo-ACs
CTRL
eMacroTAC
50µm
Annexin V
eMacroTAC (+Annexin V)
Efferocytosis index for ACs acidification (pHrodo)
p<0.0001
p=0.9980
CTRL
eMacroTAC
Annexin V
g
eMacroTAC enhances ACs binding upstreaming internalization
p<0.0001
p=0.0049
p=0.0476
Efferocytosis index for ACs binding (celltracker)
Cytochalasin D
h
eMacroTAC enhances efferocytosis dependent on peptide sequence
p=0.011
p=0.415
Efferocytosis index for ACs acidification (pHrodo)
sc-MacroTAC
100nM
1µM
i
eMacroTAC enhances the produnction of anti-inflammatory cytokines
p=0.0039
p=0.0282
p=0.0130
TGF-β (pg/mL)
Apoptotic cells
eMacroTAC
KLGFFKR
CSPGAK
GSGS
sc-MacroTAC
GLFKFRK
PSCGKA
GSGS

Fig. 1

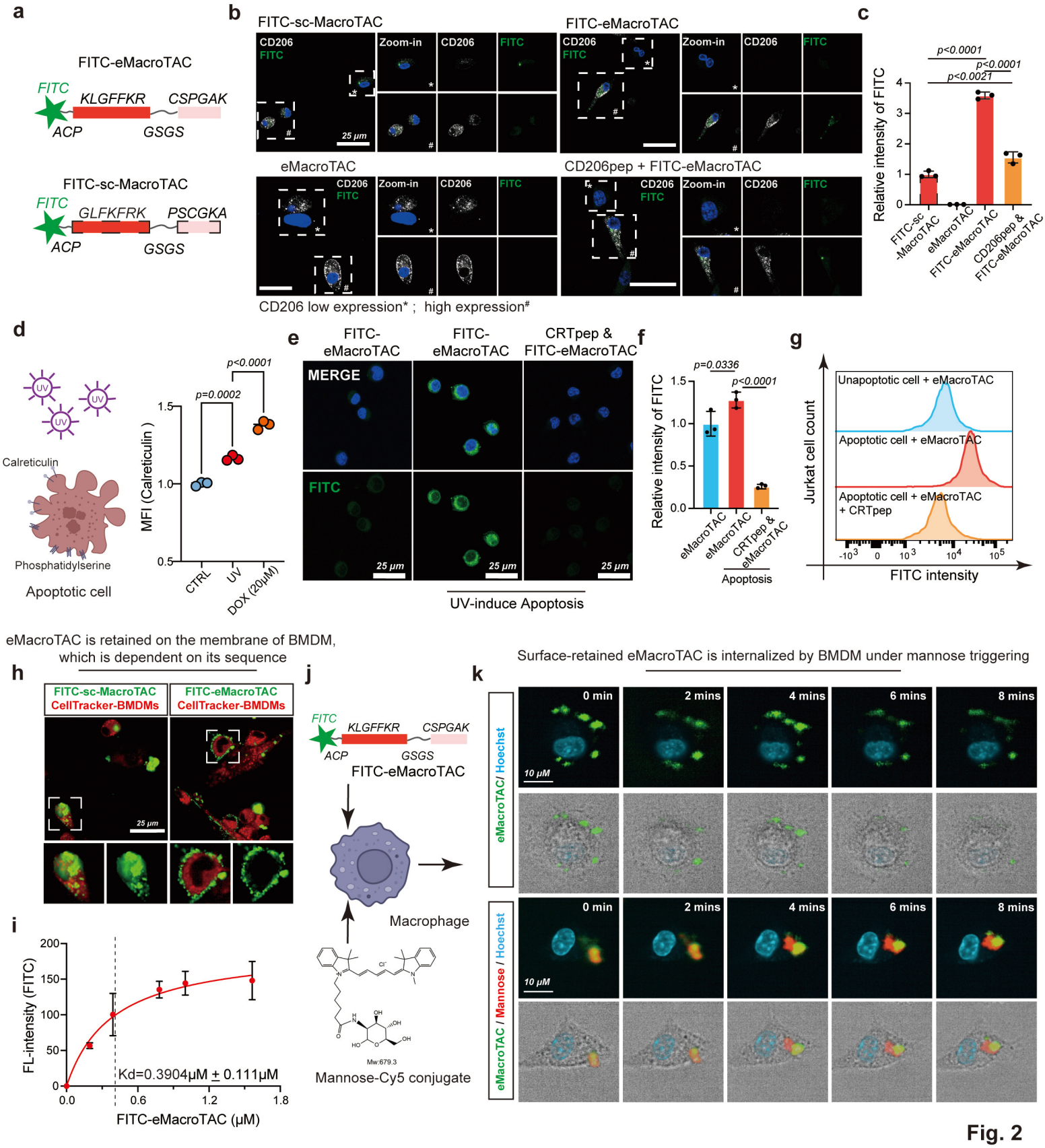
a
FITC-eMacroTAC
FITC
KLGFFKR
CSPGAK
ACP
GSGS
FITC-sc-MacroTAC
FITC
GLFKFRK
PSCGKA
ACP
GSGS
b
FITC-sc-MacroTAC
FITC-eMacroTAC
CD206
FITC
Zoom-in
25 μm
eMacroTAC
CD206pep + FITC-eMacroTAC
CD206 low expression* ; high expression#
c
Relative intensity of FITC
p<0.0001
p<0.0001
p<0.0021
FITC-sc -MacroTAC
eMacroTAC
FITC-eMacroTAC
CD206pep & FITC-eMacroTAC
d
UV
Calreticulin
Phosphatidylserine
Apoptotic cell
MFI (Calreticulin)
p<0.0001
p=0.0002
CTRL
UV
DOX (20μM)
e
FITC-eMacroTAC
FITC-eMacroTAC
CRTpep & FITC-eMacroTAC
MERGE
FITC
25 μm
UV-induce Apoptosis
f
Relative intensity of FITC
p=0.0336
p<0.0001
eMacroTAC
eMacroTAC
CRTpep & eMacroTAC
Apoptosis
g
Jurkat cell count
Unapoptotic cell + eMacroTAC
Apoptotic cell + eMacroTAC
Apoptotic cell + eMacroTAC + CRTpep
FITC intensity
eMacroTAC is retained on the membrane of BMDM, which is dependent on its sequence
h
FITC-sc-MacroTAC CellTracker-BMDMs
FITC-eMacroTAC CellTracker-BMDMs
25 μm
i
FL-intensity (FITC)
Kd=0.3904μM ± 0.111μM
FITC-eMacroTAC (μM)
j
FITC
KLGFFKR
CSPGAK
ACP
GSGS
FITC-eMacroTAC
Macrophage
Mw:679.3
Mannose-Cy5 conjugate
Surface-retained eMacroTAC is internalized by BMDM under mannose triggering
k
eMacroTAC/ Hoechst
eMacroTAC / Mannose / Hoechst
0 min
2 mins
4 mins
6 mins
8 mins
10 μM

Fig. 2

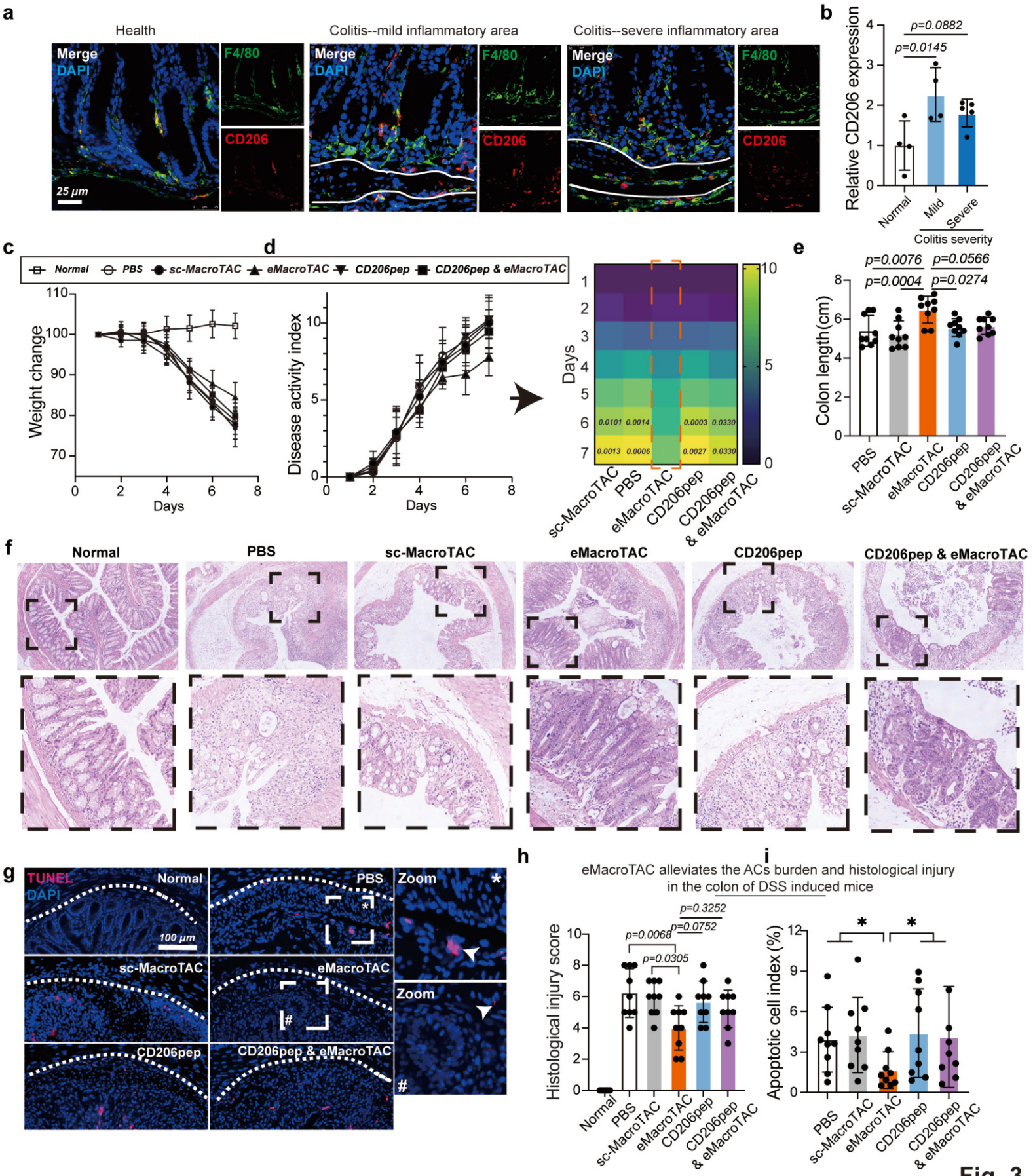
a
Health
Colitis--mild inflammatory area
Colitis--severe inflammatory area
Merge
DAPI
F4/80
CD206
25 μm
b
Relative CD206 expression
p=0.0882
p=0.0145
Normal
Mild
Severe
Colitis severity
c
Normal
PBS
sc-MacroTAC
eMacroTAC
CD206pep
CD206pep & eMacroTAC
Weight change
Days
d
Disease activity index
Days
Days
0.0101
0.0014
0.0003
0.0330
0.0013
0.0006
0.0027
0.0330
sc-MacroTAC
PBS
eMacroTAC
CD206pep
CD206pep & eMacroTAC
e
Colon length(cm)
p=0.0076
p=0.0566
p=0.0004
p=0.0274
PBS
sc-MacroTAC
eMacroTAC
CD206pep
CD206pep & eMacroTAC
f
Normal
PBS
sc-MacroTAC
eMacroTAC
CD206pep
CD206pep & eMacroTAC
g
TUNEL
DAPI
Normal
PBS
Zoom
100 μm
sc-MacroTAC
eMacroTAC
Zoom
CD206pep
CD206pep & eMacroTAC
h
Histological injury score
p=0.3252
p=0.0752
p=0.0068
p=0.0305
Normal
PBS
sc-MacroTAC
eMacroTAC
CD206pep
CD206pep & eMacroTAC
i
eMacroTAC alleviates the ACs burden and histological injury in the colon of DSS induced mice
Apoptotic cell index (%)
PBS
sc-MacroTAC
eMacroTAC
CD206pep
CD206pep & eMacroTAC

Fig. 3

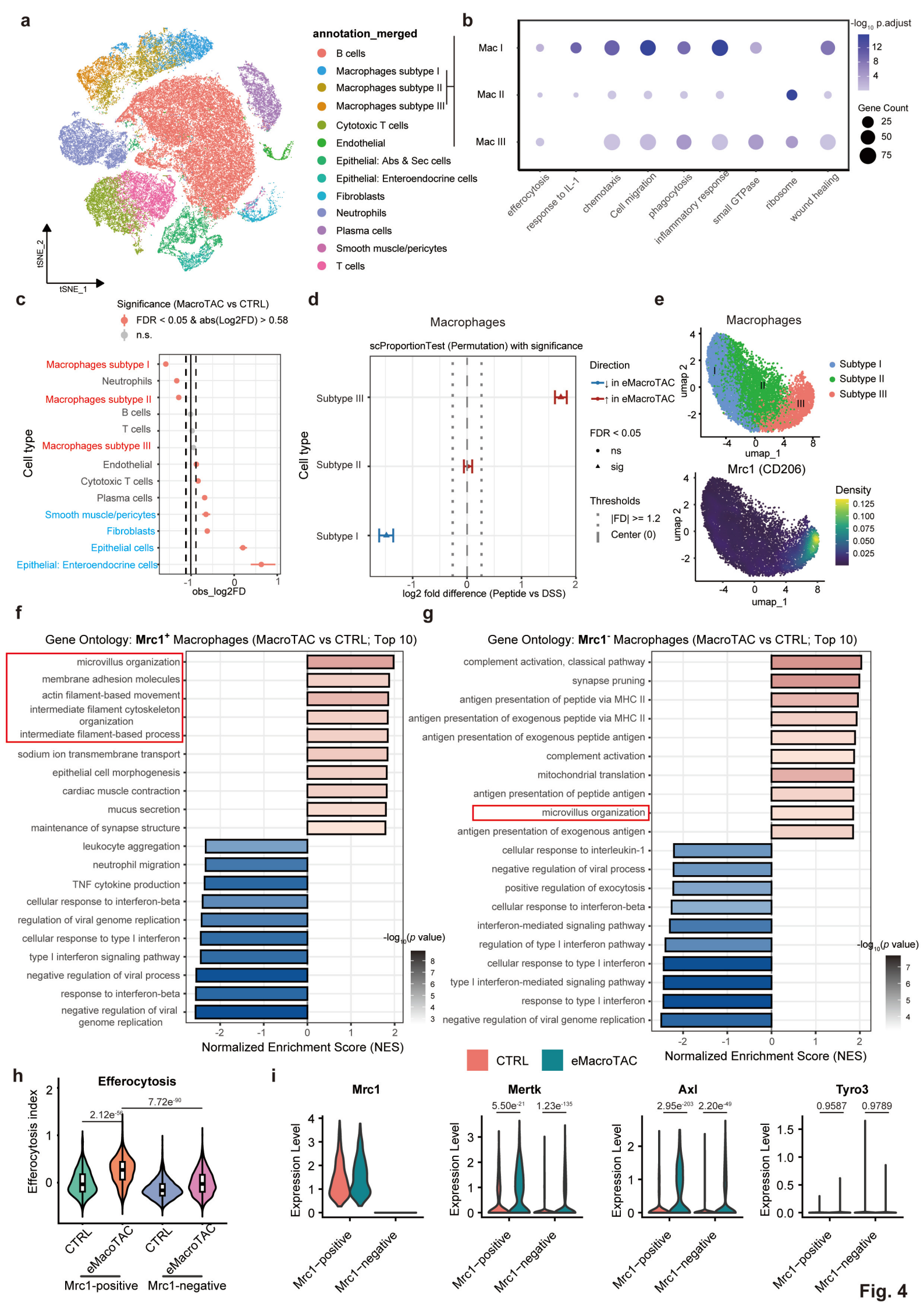
a
annotation_merged
B cells
Macrophages subtype I
Macrophages subtype II
Macrophages subtype III
Cytotoxic T cells
Endothelial
Epithelial: Abs & Sec cells
Epithelial: Enteroendocrine cells
Fibroblasts
Neutrophils
Plasma cells
Smooth muscle/pericytes
T cells
tSNE_2
tSNE_1
b
Mac I
Mac II
Mac III
-log10 p.adjust
Gene Count
efferocytosis
response to IL-1
chemotaxis
Cell migration
phagocytosis
inflammatory response
small GTPase
ribosome
wound healing
c
Significance (MacroTAC vs CTRL)
FDR < 0.05 & abs(Log2FD) > 0.58
n.s.
Cell type
obs_log2FD
d
Macrophages
scProportionTest (Permutation) with significance
Subtype III
Subtype II
Subtype I
log2 fold difference (Peptide vs DSS)
Direction
↓ in eMacroTAC
↑ in eMacroTAC
FDR < 0.05
ns
sig
Thresholds
|FD| >= 1.2
Center (0)
e
Macrophages
umap_1
umap 2
Subtype I
Subtype II
Subtype III
Mrc1 (CD206)
Density
f
Gene Ontology: Mrc1+ Macrophages (MacroTAC vs CTRL; Top 10)
microvillus organization
membrane adhesion molecules
actin filament-based movement
intermediate filament cytoskeleton organization
intermediate filament-based process
sodium ion transmembrane transport
epithelial cell morphogenesis
cardiac muscle contraction
mucus secretion
maintenance of synapse structure
leukocyte aggregation
neutrophil migration
TNF cytokine production
cellular response to interferon-beta
regulation of viral genome replication
cellular response to type I interferon
type I interferon signaling pathway
negative regulation of viral process
response to interferon-beta
negative regulation of viral genome replication
-log10(p value)
Normalized Enrichment Score (NES)
g
Gene Ontology: Mrc1- Macrophages (MacroTAC vs CTRL; Top 10)
complement activation, classical pathway
synapse pruning
antigen presentation of peptide via MHC II
antigen presentation of exogenous peptide via MHC II
antigen presentation of exogenous peptide antigen
complement activation
mitochondrial translation
antigen presentation of peptide antigen
microvillus organization
antigen presentation of exogenous antigen
cellular response to interleukin-1
negative regulation of viral process
positive regulation of exocytosis
cellular response to interferon-beta
interferon-mediated signaling pathway
regulation of type I interferon pathway
cellular response to type I interferon
type I interferon-mediated signaling pathway
response to type I interferon
negative regulation of viral genome replication
-log10(p value)
Normalized Enrichment Score (NES)
CTRL
eMacroTAC
h
Efferocytosis
Efferocytosis index
2.12e-56
7.72e-90
CTRL
eMacoTAC
CTRL
eMacroTAC
Mrc1-positive
Mrc1-negative
i
Mrc1
Mertk
Axl
Tyro3
Expression Level
5.50e-21
1.23e-135
2.95e-203
2.20e-49
0.9587
0.9789
Mrc1−positive
Mrc1−negative

Fig. 4

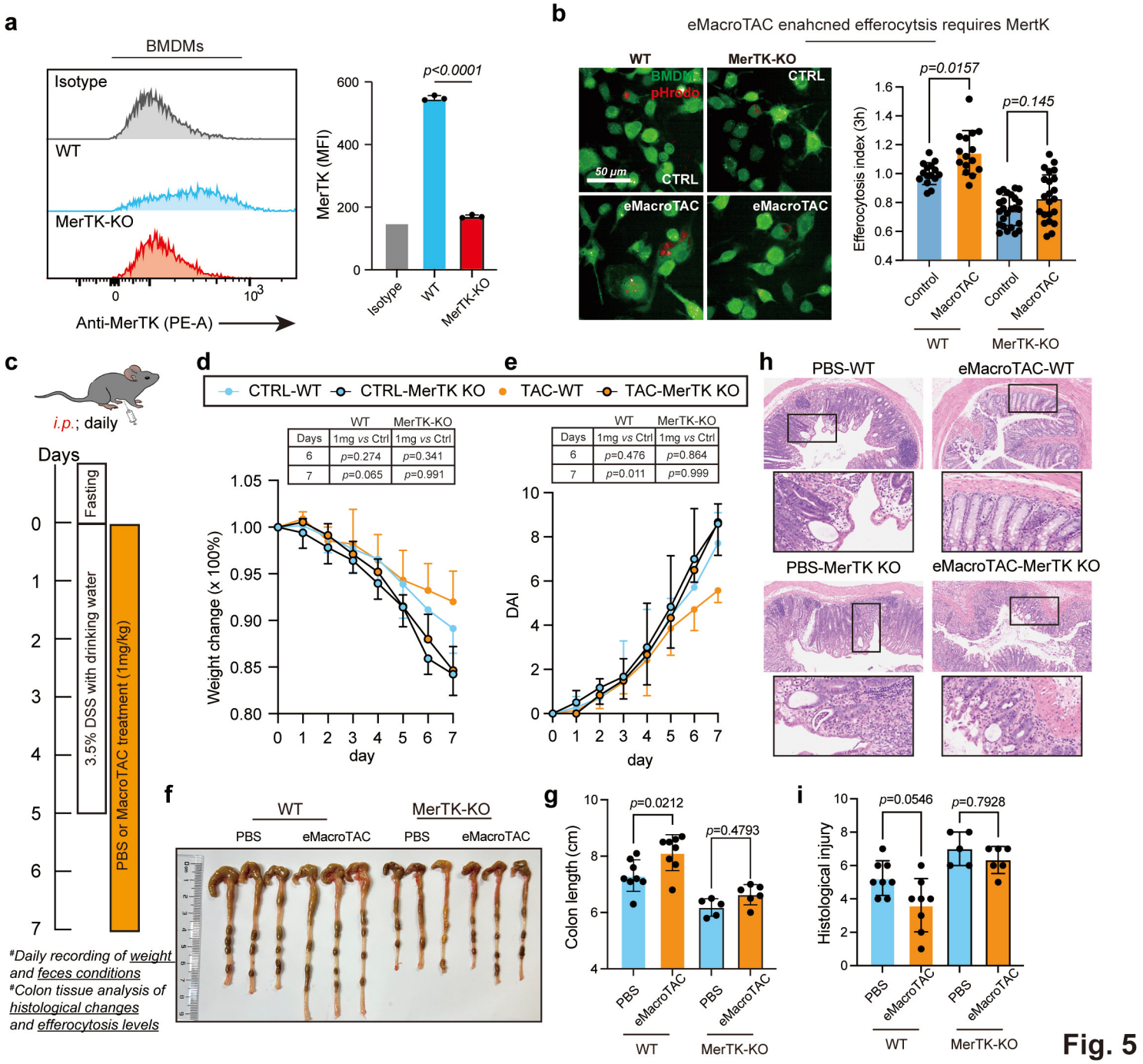

Days	WT 1mg *vs* Ctrl	MerTK-KO 1mg *vs* Ctrl
6	*p*=0.274	*p*=0.341
7	*p*=0.065	*p*=0.991

Days	WT 1mg *vs* Ctrl	MerTK-KO 1mg *vs* Ctrl
6	*p*=0.476	*p*=0.864
7	*p*=0.011	*p*=0.999

Fig. 5

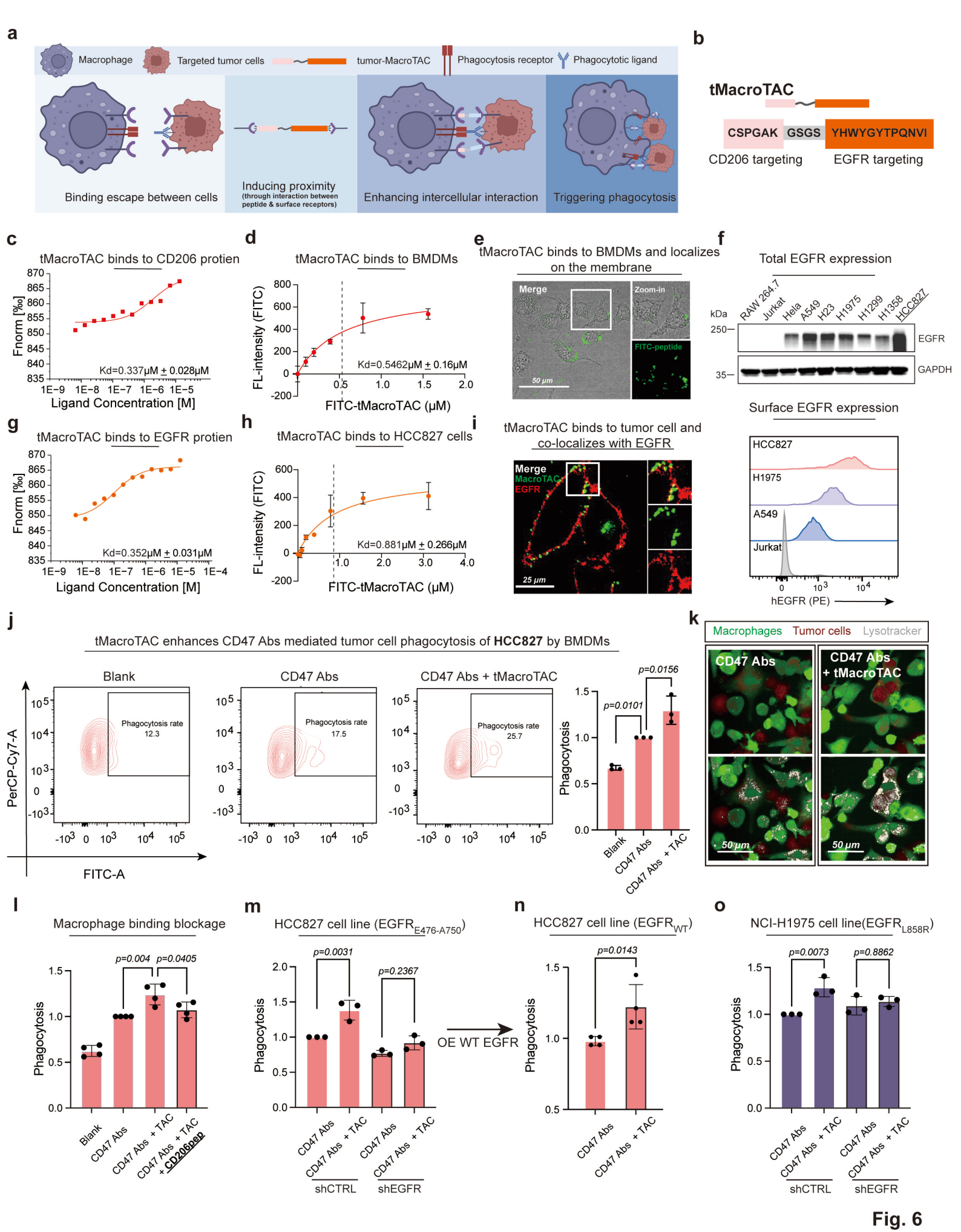
a
Macrophage
Targeted tumor cells
tumor-MacroTAC
Phagocytosis receptor
Phagocytotic ligand
Binding escape between cells
Inducing proximity
(through interaction between peptide & surface receptors)
Enhancing intercellular interaction
Triggering phagocytosis
b
tMacroTAC
CSPGAK
GSGS
YHWYGYTPQNVI
CD206 targeting
EGFR targeting
c
tMacroTAC binds to CD206 protien
Fnorm [‰]
Kd=0.337μM ± 0.028μM
Ligand Concentration [M]
d
tMacroTAC binds to BMDMs
FL-intensity (FITC)
Kd=0.5462μM ± 0.16μM
FITC-tMacroTAC (μM)
e
tMacroTAC binds to BMDMs and localizes on the membrane
Merge
Zoom-in
FITC-peptide
50 μm
f
Total EGFR expression
kDa
RAW 264.7
Jurkat
Hela
A549
H23
H1975
H1299
H1358
HCC827
250—
35—
EGFR
GAPDH
Surface EGFR expression
HCC827
H1975
A549
Jurkat
hEGFR (PE)
g
tMacroTAC binds to EGFR protien
Fnorm [‰]
Kd=0.352μM ± 0.031μM
Ligand Concentration [M]
h
tMacroTAC binds to HCC827 cells
FL-intensity (FITC)
Kd=0.881μM ± 0.266μM
FITC-tMacroTAC (μM)
i
tMacroTAC binds to tumor cell and co-localizes with EGFR
Merge
MacroTAC
EGFR
25 μm
j
tMacroTAC enhances CD47 Abs mediated tumor cell phagocytosis of HCC827 by BMDMs
Blank
CD47 Abs
CD47 Abs + tMacroTAC
Phagocytosis rate
12.3
17.5
25.7
PerCP-Cy7-A
FITC-A
Phagocytosis
p=0.0101
p=0.0156
Blank
CD47 Abs
CD47 Abs + TAC
k
Macrophages
Tumor cells
Lysotracker
CD47 Abs
CD47 Abs + tMacroTAC
50 μm
l
Macrophage binding blockage
p=0.004
p=0.0405
Phagocytosis
Blank
CD47 Abs
CD47 Abs + TAC
CD47 Abs + TAC + CD206pep
m
HCC827 cell line (EGFR E476-A750)
p=0.0031
p=0.2367
Phagocytosis
CD47 Abs
CD47 Abs + TAC
shCTRL
shEGFR
OE WT EGFR
n
HCC827 cell line (EGFR WT)
p=0.0143
Phagocytosis
CD47 Abs
CD47 Abs + TAC
o
NCI-H1975 cell line(EGFR L858R)
p=0.0073
p=0.8862
Phagocytosis
CD47 Abs
CD47 Abs + TAC
shCTRL
shEGFR

Fig. 6

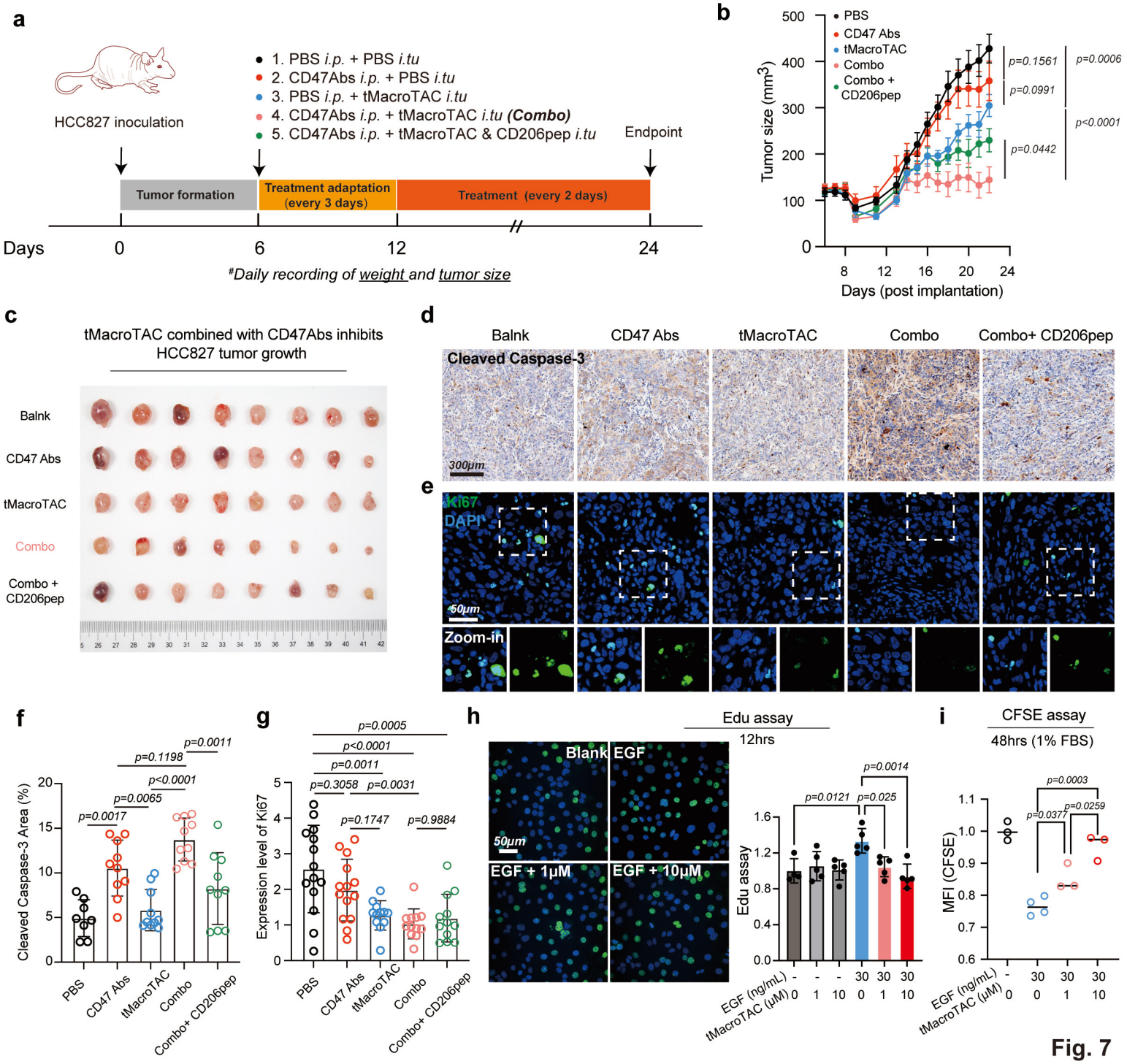
a
HCC827 inoculation
1. PBS i.p. + PBS i.tu
2. CD47Abs i.p. + PBS i.tu
3. PBS i.p. + tMacroTAC i.tu
4. CD47Abs i.p. + tMacroTAC i.tu (Combo)
5. CD47Abs i.p. + tMacroTAC & CD206pep i.tu
Endpoint
Tumor formation
Treatment adaptation (every 3 days)
Treatment (every 2 days)
Days 0 6 12 24
#Daily recording of weight and tumor size
b
PBS
CD47 Abs
tMacroTAC
Combo
Combo + CD206pep
Tumor size (mm3)
Days (post implantation)
p=0.1561
p=0.0006
p=0.0991
p<0.0001
p=0.0442
c
tMacroTAC combined with CD47Abs inhibits HCC827 tumor growth
Balnk
CD47 Abs
tMacroTAC
Combo
Combo + CD206pep
d
Balnk
CD47 Abs
tMacroTAC
Combo
Combo+ CD206pep
Cleaved Caspase-3
300μm
e
Ki67
DAPI
50μm
Zoom-in
f
Cleaved Caspase-3 Area (%)
p=0.0017
p=0.1198
p=0.0065
p<0.0001
p=0.0011
PBS
CD47 Abs
tMacroTAC
Combo
Combo+ CD206pep
g
Expression level of Ki67
p=0.0005
p<0.0001
p=0.0011
p=0.3058
p=0.0031
p=0.1747
p=0.9884
h
Edu assay
12hrs
Blank
EGF
EGF + 1μM
EGF + 10μM
50μm
Edu assay
p=0.0014
p=0.0121
p=0.025
EGF (ng/mL)
tMacroTAC (μM)
i
CFSE assay
48hrs (1% FBS)
MFI (CFSE)
p=0.0003
p=0.0259
p=0.0377
EGF (ng/mL)
tMacroTAC (μM)

Fig. 7

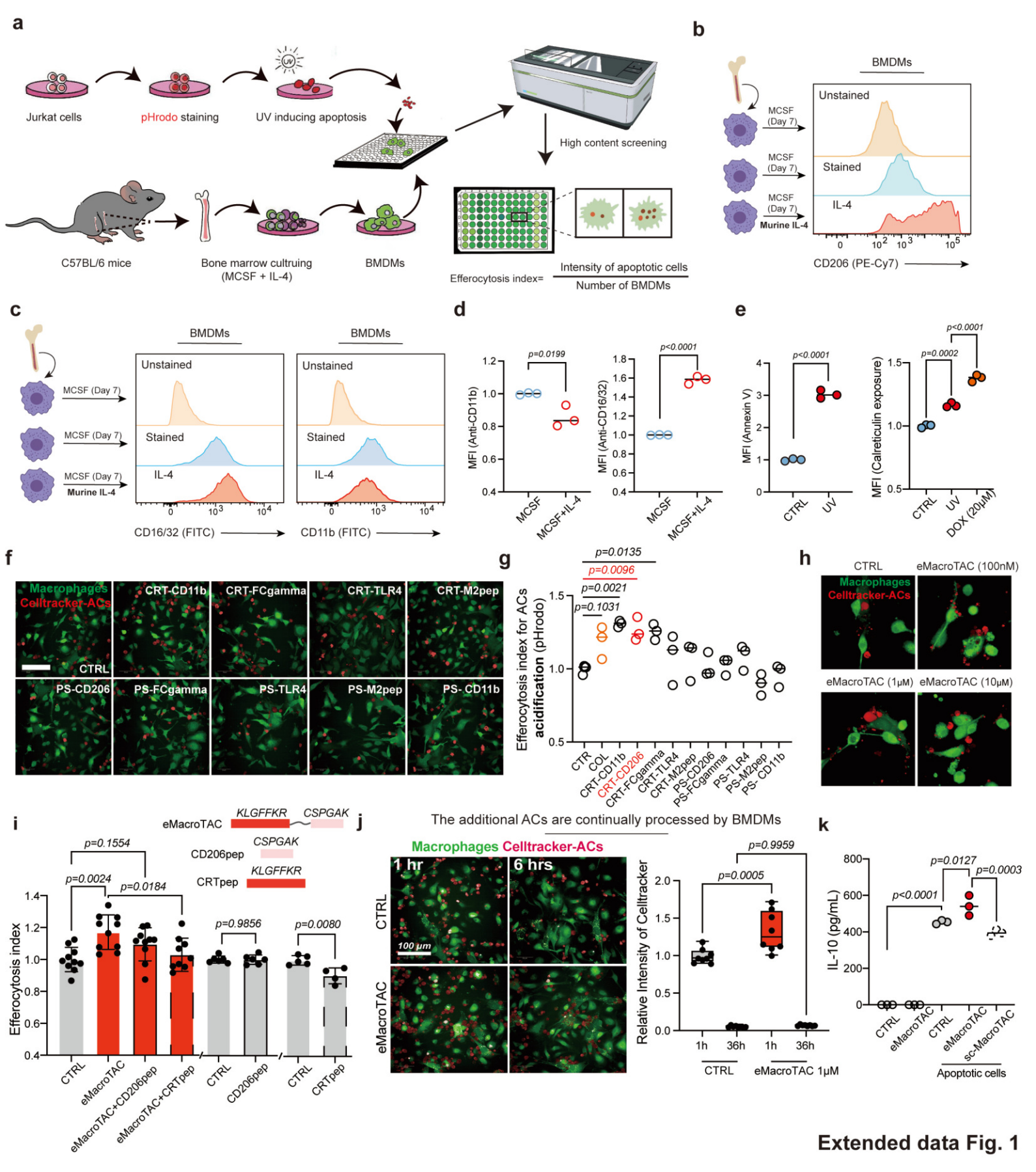

Extended data Fig. 1

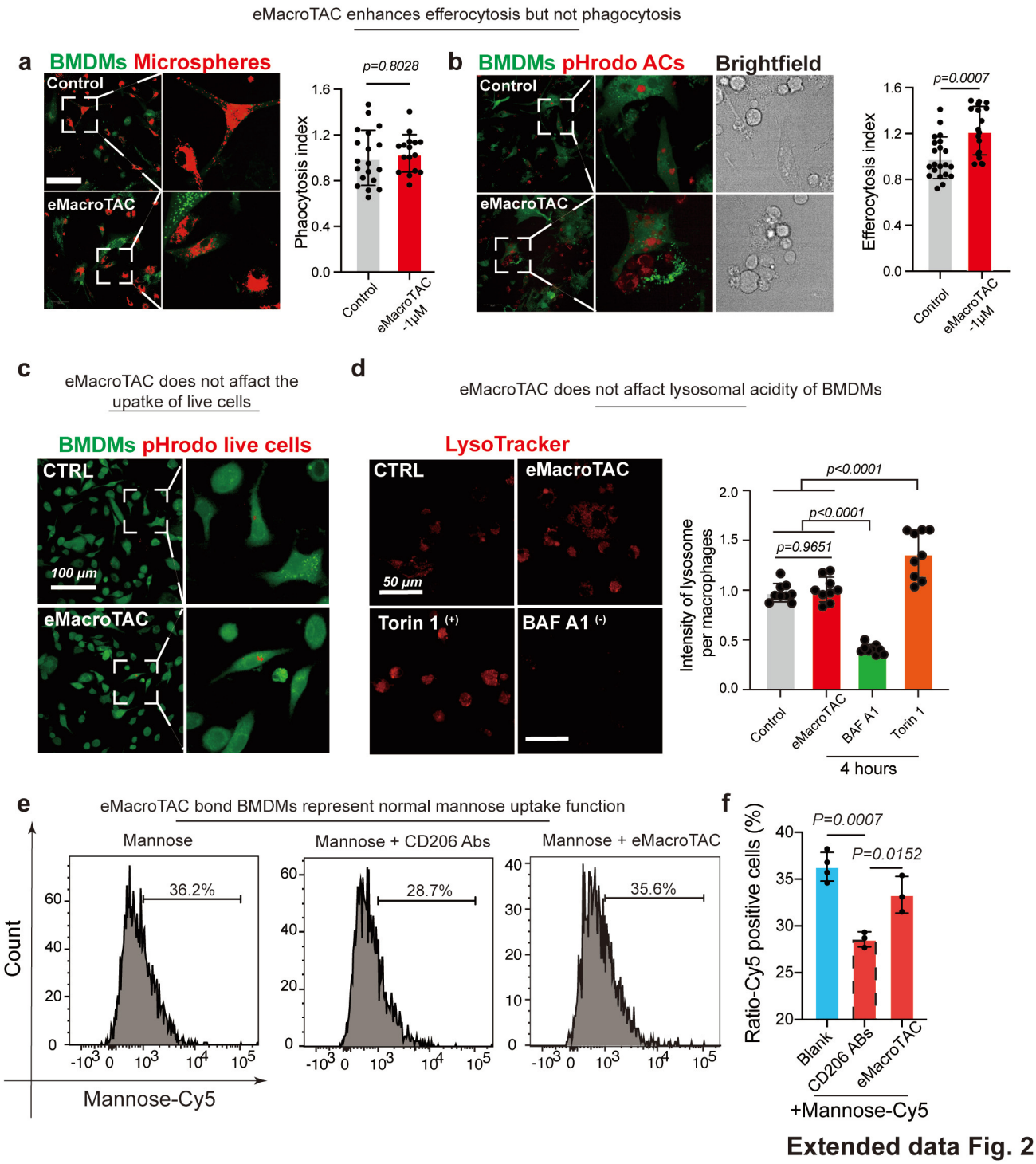

Extended data Fig. 2

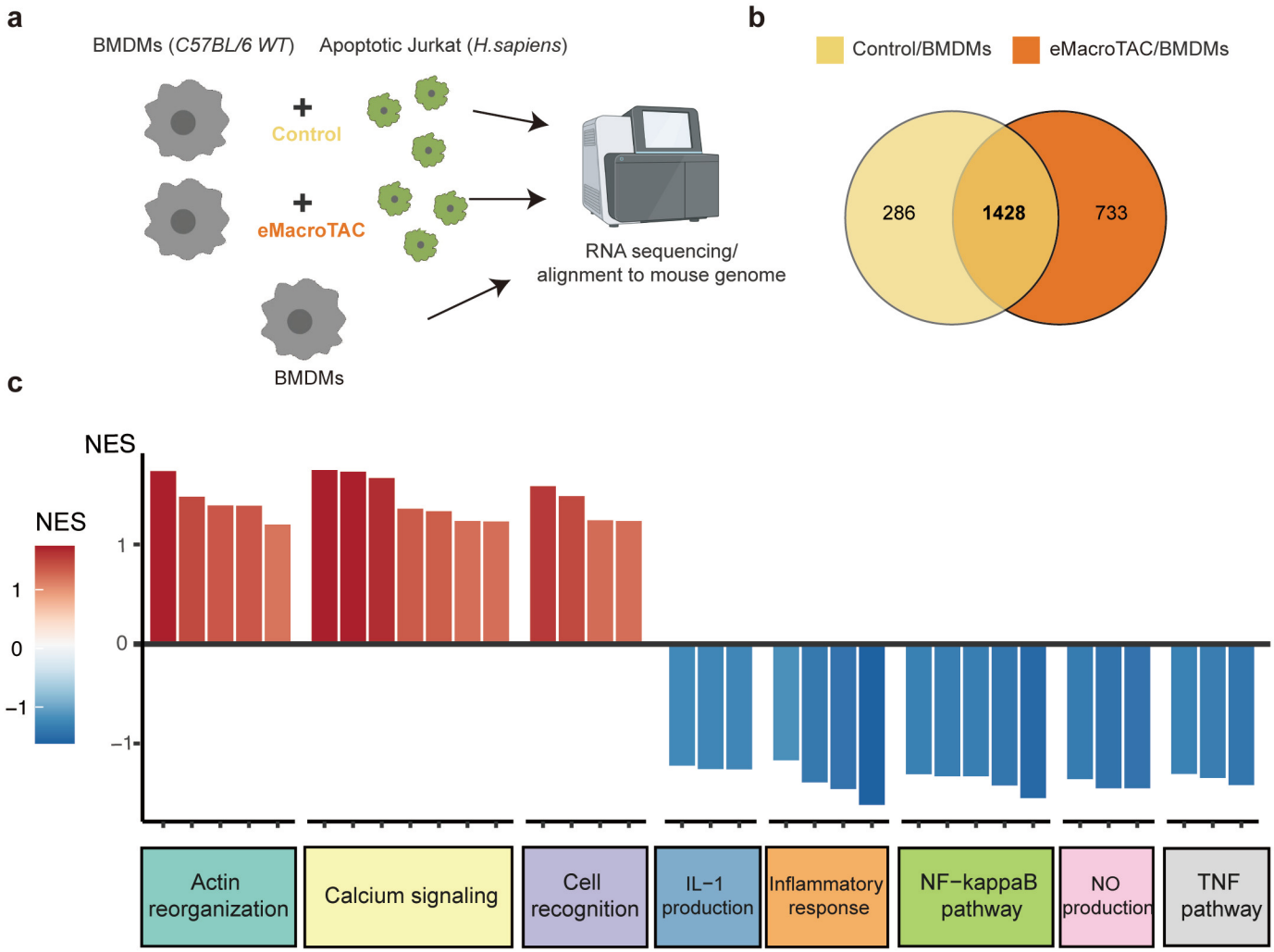

Extended data Fig. 3

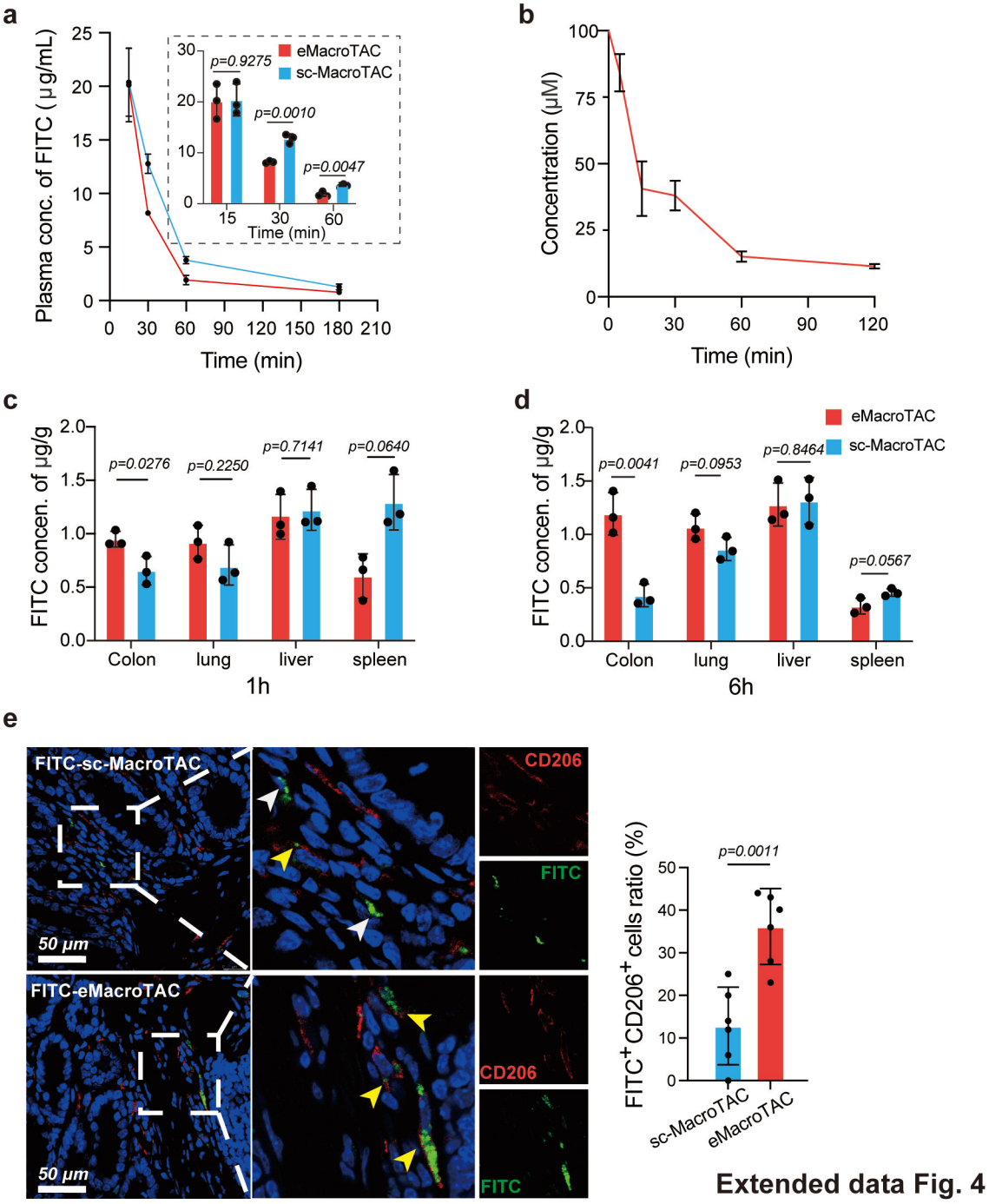

Extended data Fig. 4

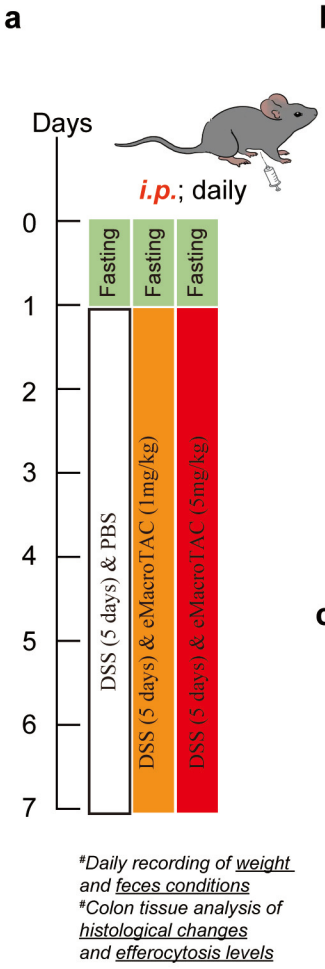

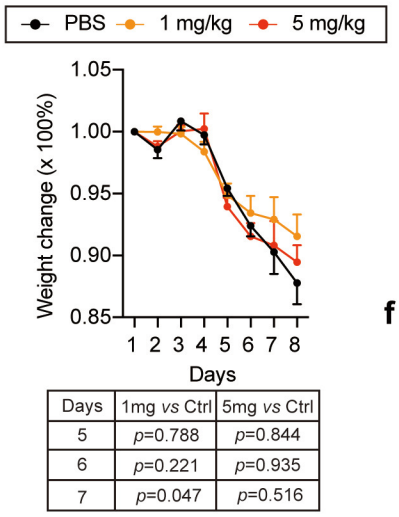

Days	1mg *vs* Ctrl	5mg *vs* Ctrl
5	*p*=0.788	*p*=0.844
6	*p*=0.221	*p*=0.935
7	*p*=0.047	*p*=0.516

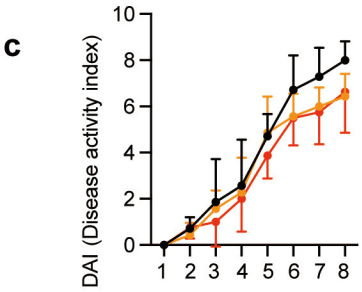

Days	1mg *vs* Ctrl	5mg *vs* Ctrl
5	*p*=0.157	*p*=0.108
6	*p*=0.097	*p*=0.030
7	*p*=0.032	*p*=0.059

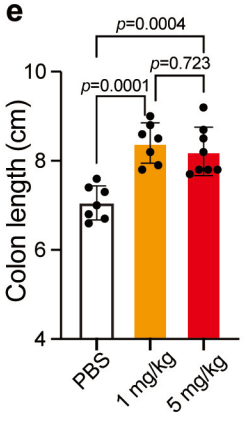

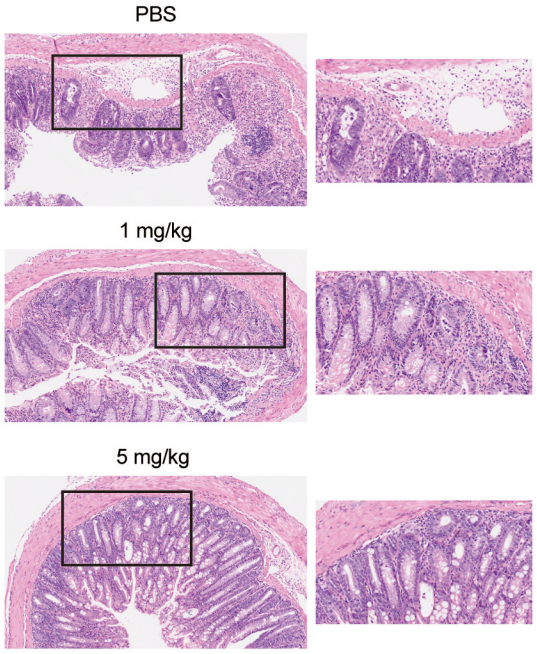

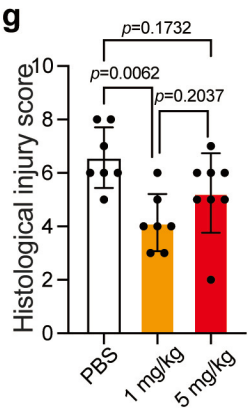

Extended data Fig. 5

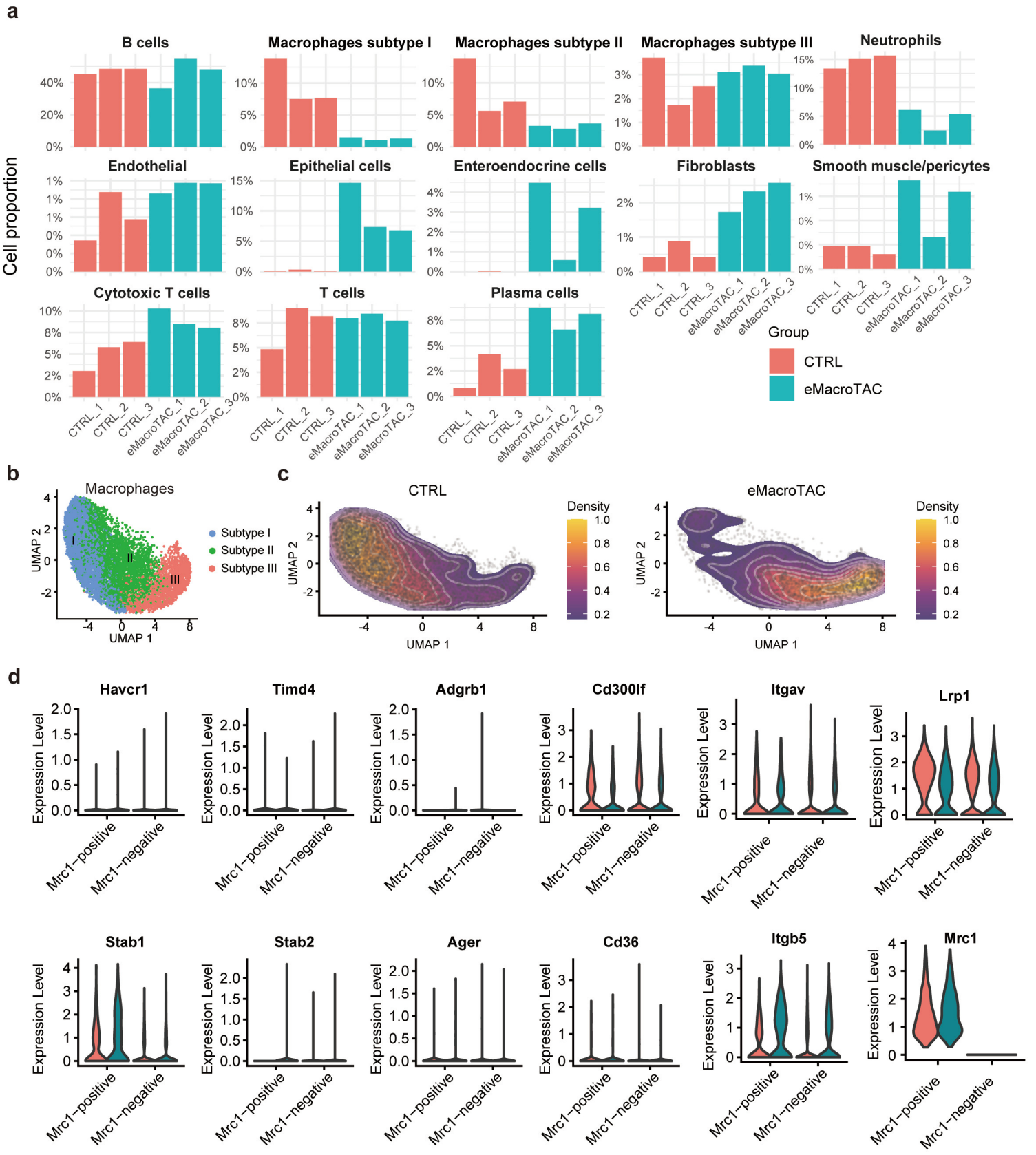

Extended data Fig. 6

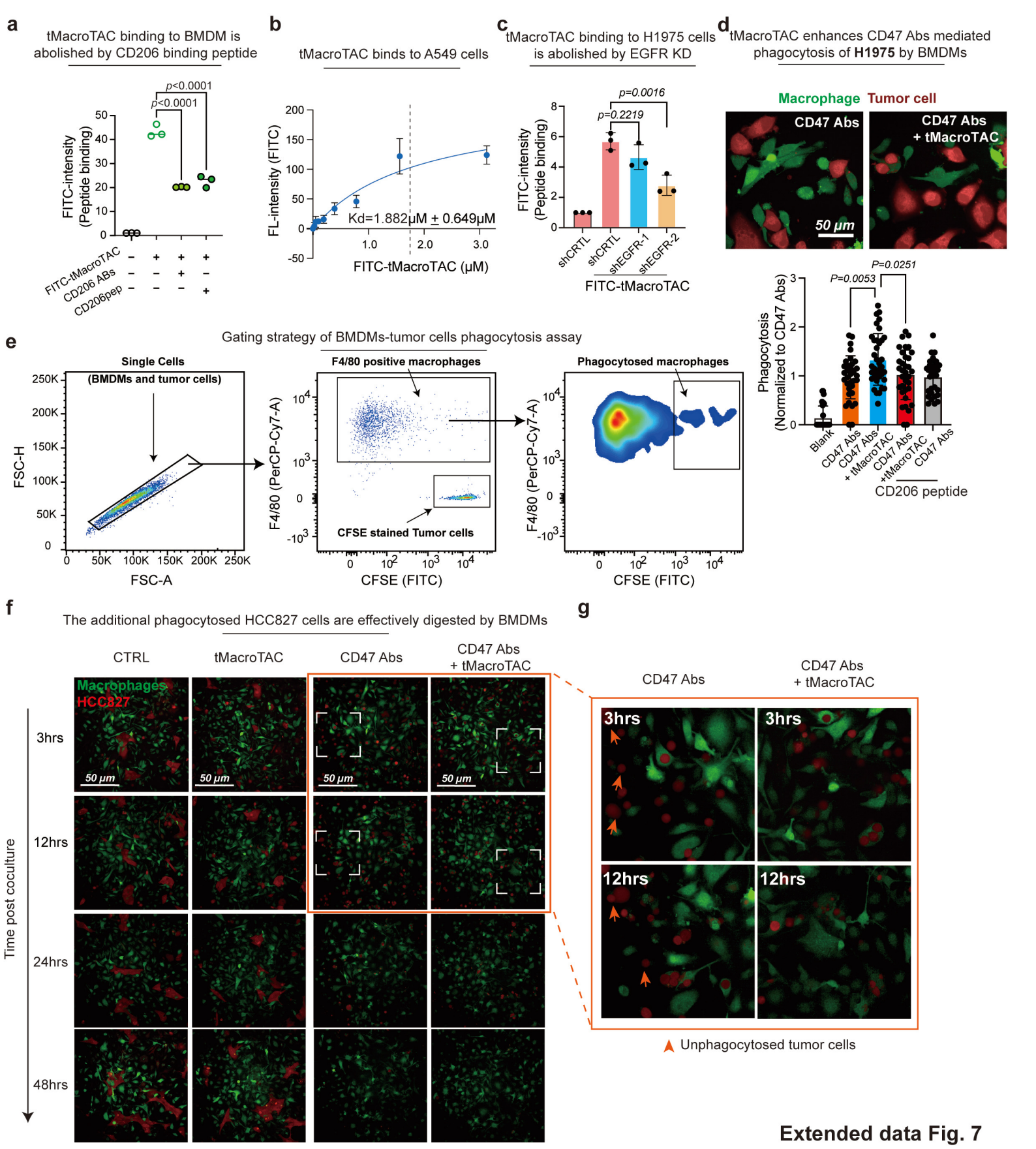

Extended data Fig. 7

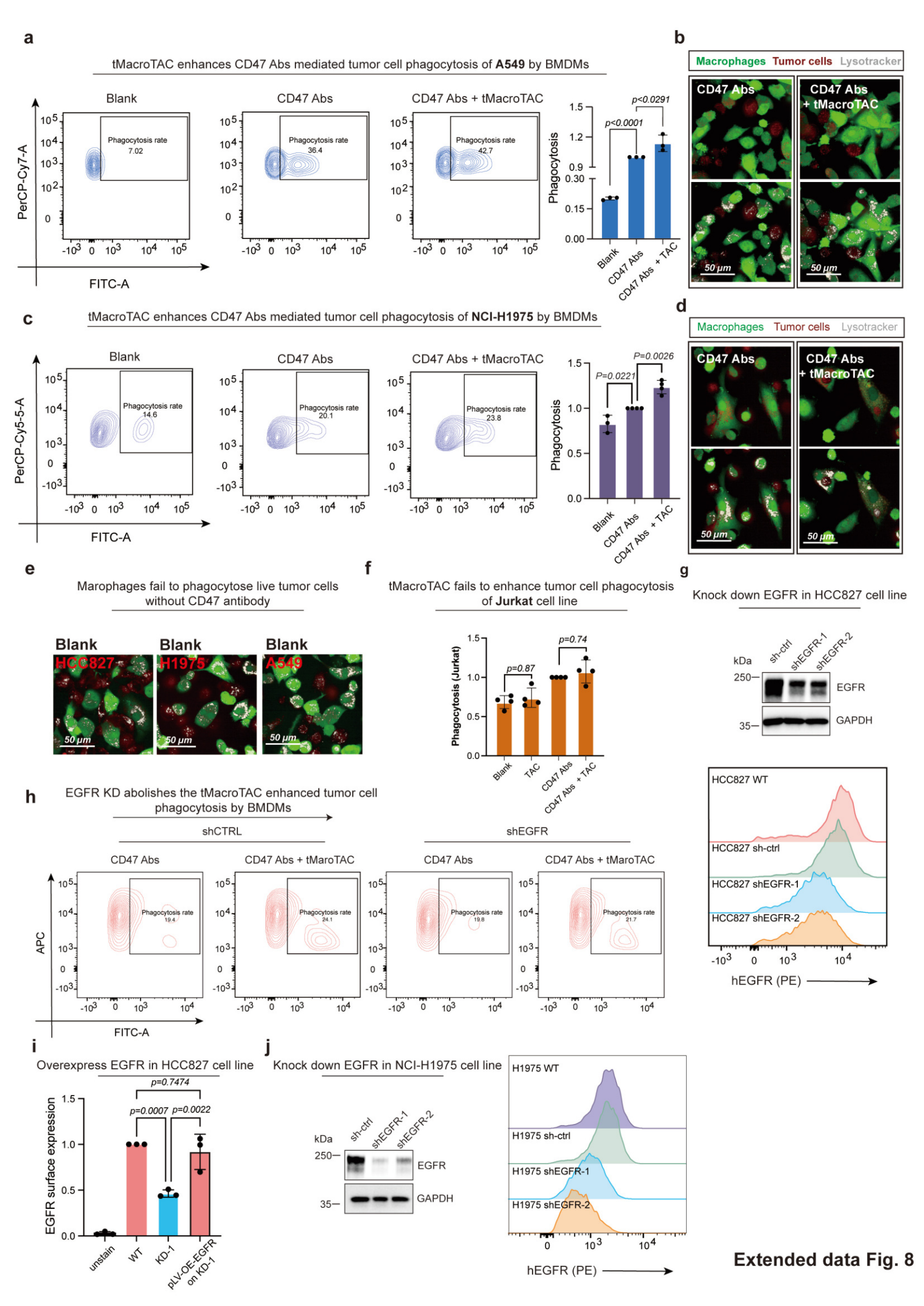

Extended data Fig. 8

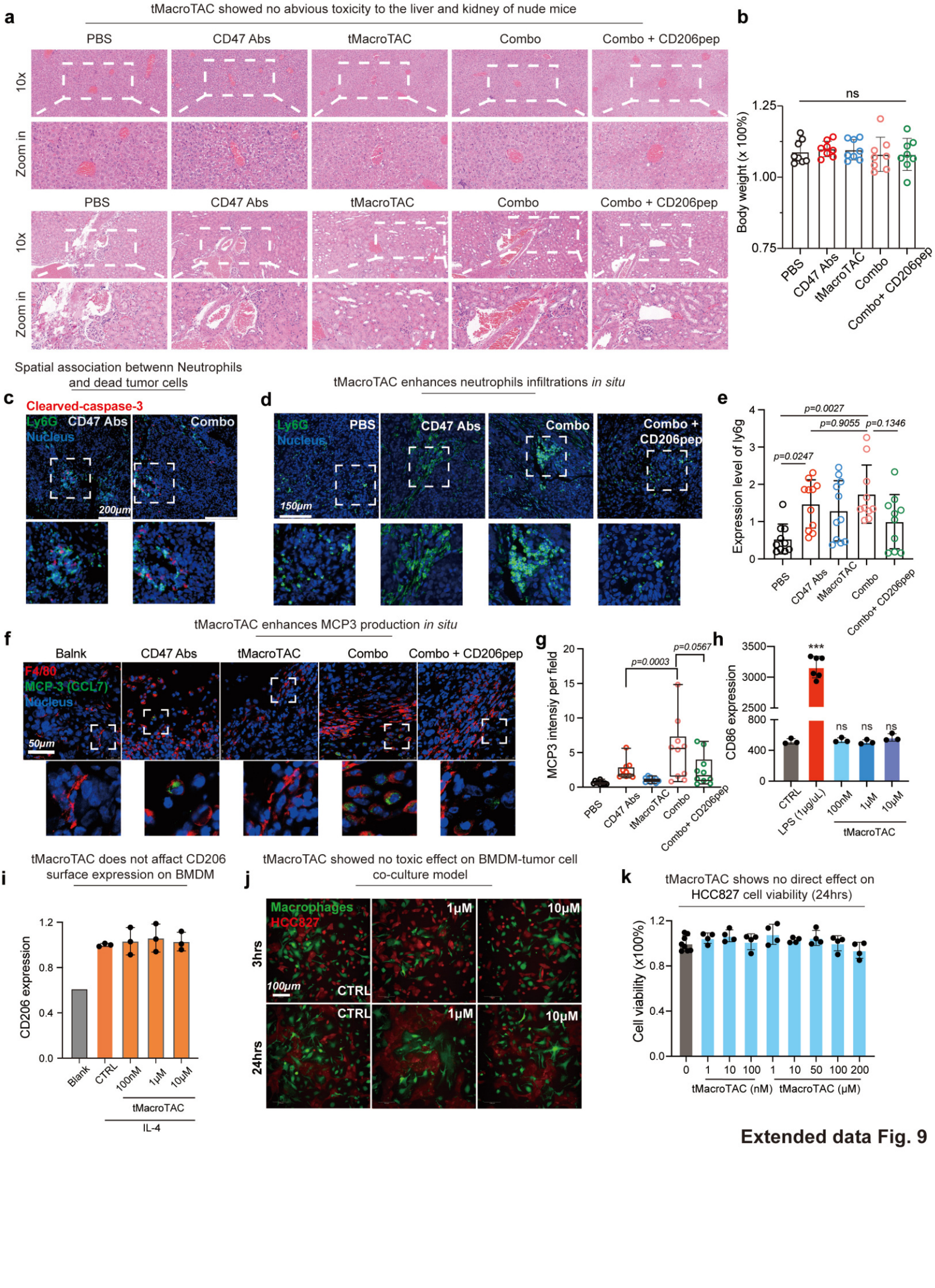

Extended data Fig. 9

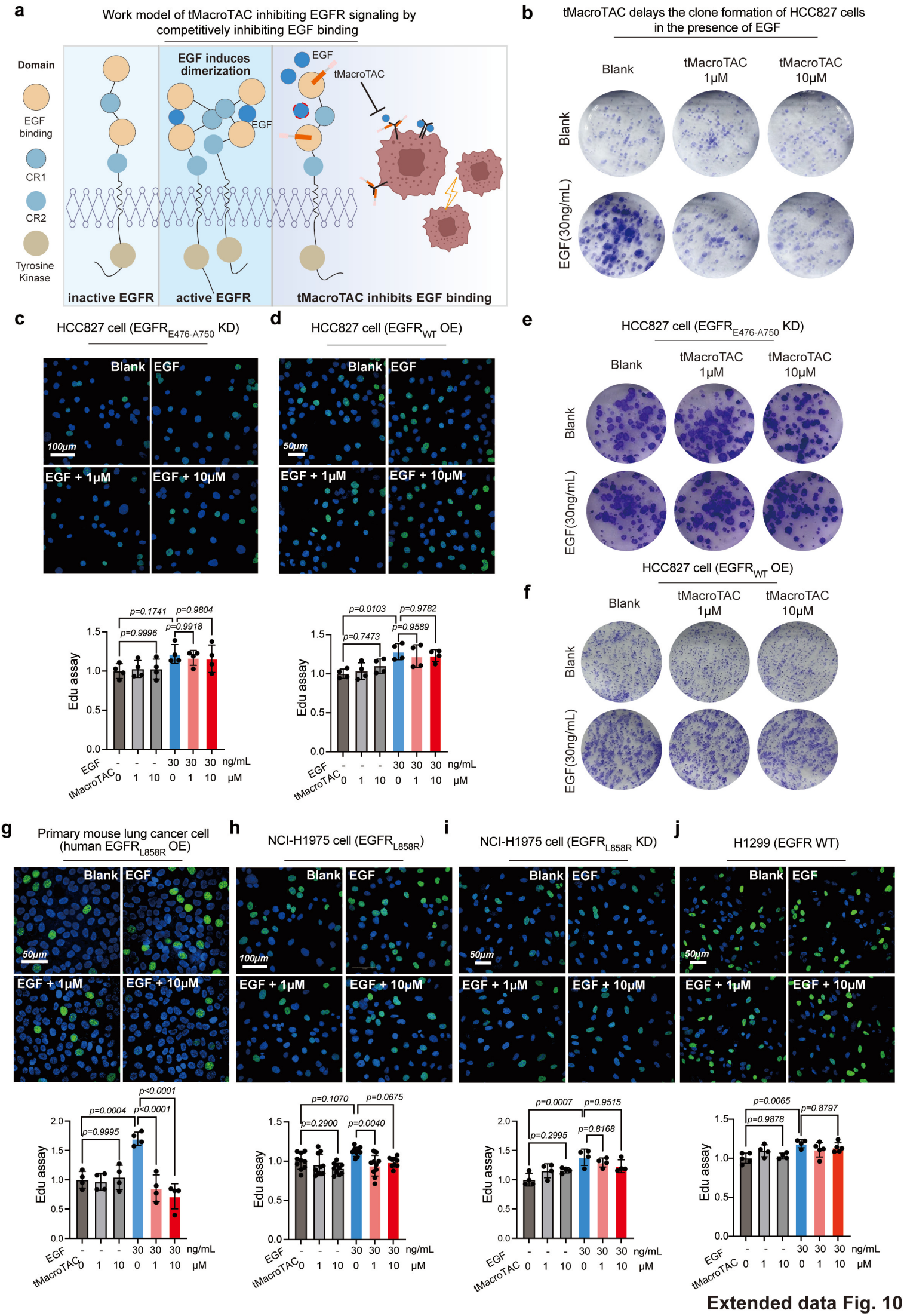

Extended data Fig. 10